Summer 8-11-2021

INFLUENCE OF POSTERIOR ELEMENTS ON THE CORRELATIONS BETWEEN MICROARCHITECTURE PARAMETERS OF TRABECULAR BONE AND STOCHASTIC PREDICTORS FROM THE DXA SCANS OF HUMAN LUMBAR VERTEBRAE

Indu Reddy Enukonda
University of Texas at Tyler

INFLUENCE OF POSTERIOR ELEMENTS ON THE CORRELATIONS BETWEEN MICROARCHITECTURE PARAMETERS OF TRABECULAR BONE AND STOCHASTIC PREDICTORS FROM THE DXA SCANS OF HUMAN LUMBAR VERTEBRAE

by

INDU REDDY ENUKONDA

A thesis submitted in partial fulfillment
of the requirements for the degree of
Master of Science in Kinesiology
Department of Health and Kinesiology

X. Neil Dong, Ph.D., Committee Chair

College of Nursing and Health Sciences

The University of Texas at Tyler
July 2021

POSTERIOR ELEMENTS OF HUMAN LUMBAR VERTEBRAE

The University of Texas at Tyler

Tyler, Texas

This is to certify that the Master's Thesis of

Indu Reddy Enukonda

has been approved for the thesis requirement on
July 6, 2021
for the Master of Science in Kinesiology degree

Approvals:

DocuSigned by:
X. Neil Dong
3F9490B76924422...
Thesis Chair: X. Neil Dong, Ph.D.

DocuSigned by:
3BC8CB40452F485...
Member: Scott Spier, Ph.D.

DocuSigned by:
Mukul Shirvaikar
A6F668C6680B49A...
Member: Mukul Shirvaikar, Ph.D.

DocuSigned by:
David Criswell
F977514BAC7417...
David Criswell, Ph.D.
Chair, Department of Health and Kinesiology

DocuSigned by:
Barbara Haas
985A922F3BF54C7...
Barbara Haas, Ph.D.
Interim Dean, College of Nursing and Health Sciences

Acknowledgments

Firstly, my sincere and heartful thanks and appreciation to my advisor Professor Dr. X. Neil Dong, for the constant help throughout the process. From teaching basics to helping me to evolve as a researcher, it wouldn't be possible. Thank you once again for all your advice and suggestions. I would also like to thank my committee members, professors Dr. Scott Spier and Dr. Mukul Shirvaikar for their guidance, support, and help.

Special thanks to my family and friends for their support. Without whom I wouldn't be able to sustain this far. Thank you once again for all who helped me in this process and made me achieve my goals.

Table of Contents

List of Tables

List of Figures

ABSTRACT

INFLUENCE OF POSTERIOR ELEMENTS ON THE CORRELATIONS BETWEEN MICROARCHITECTURE PARAMETERS OF TRABECULAR BONE AND STOCHASTIC PREDICTORS FROM THE DXA SCANS OF HUMAN LUMBAR VERTEBRAE

Indu Reddy Enukonda

Thesis Chair: X. Neil Dong, Ph.D.

The University of Texas at Tyler

August 2021

Osteoporosis is a bone disease affecting both postmenopausal women and older men. Bone fractures caused by osteoporosis are a major health concern, creating a great economic burden to our society. Bone mineral density (BMD), a measure of bone mass by Dual-energy X-ray Absorptiometry (DXA), is a major risk factor for bone fractures. In addition to BMD, trabecular microarchitecture also contributes to bone strength and therefore is a risk factor for osteoporotic fractures. Recently, stochastic predictors derived from DXA scans have been found to correlate with trabecular microarchitecture in human vertebrae. In routine clinical scans of the human lumbar spine, posterior elements are always included during the posterior-anterior (PA) projection of DXA scans. To our knowledge, the influence of posterior elements on the relationship between stochastic predictors and trabecular microarchitecture has not been investigated. Therefore, the objective of this study is to examine the effect of posterior elements on the estimation of stochastic predictors using simulated DXA scans.

POSTERIOR ELEMENTS OF HUMAN LUMBAR VERTEBRAE

3D MicroCT images of human vertebrae from the lumbar spine of five tissue donors were obtained. Simulated DXA images of human vertebrae with and without posterior elements were generated from these 3D MicroCT images. Stochastic parameters such as correlation length and sill variance were calculated by fitting a theoretical model onto the experimental variogram of simulated DXA images. Linear regression analyses were performed to examine the correlations between microarchitecture of trabecular bone and stochastic predictors from DXA images of human vertebrae with and without posterior elements.

The sill variance of simulated DXA images without posterior elements was positively correlated with some of the microarchitecture parameters such as bone surface to volume ratio, trabecular separation, and negatively correlated with bone volume fraction, trabecular thickness, trabecular number. The sill variance of simulated DXA images of whole vertebrae was positively correlated with bone volume fraction, trabecular thickness, trabecular number, and connectivity density, and negatively correlated with the bone surface to volume ratio, trabecular separation. Although these correlations were not statistically significant, the correlations between the sill variance and microarchitecture parameters were mostly greater in the vertebral body without posterior elements than the whole vertebrae with intact posterior elements.

The outcome of this study indicates that it is necessary to remove posterior elements from DXA scans of the lumbar spine to improve the prediction of bone fractures using stochastic predictors.

Chapter 1

INTRODUCTION

Osteoporosis and Fragility Fractures

Definition of Osteoporosis

Osteoporosis is a bone disease characterized by low bone mass, bone tissue deterioration, and disruption of bone microarchitecture which leads to loss of bone strength and makes us vulnerable to bone fractures (Sozen et al., 2017).

Epidemiology and population statistics, Health costs, and Economic costs

Diagnosis of osteoporosis during the initial stages is vital for early intervention. The treatment includes osteoporotic drugs but the medical cost for osteoporosis-related fracture, pain, and disability are extensive and it is going to increase as individual ages (Wang et al., 2015). In the U.S., it is estimated that around 8.2 million women and 2.0 million men had osteoporosis and an additional 27.3 million women, and 16.1 million men had osteopenia, a precursor to osteoporosis (Wright et al., 2014). According to the International Osteoporosis Foundation, every 1 in 3 women over the age of 50 and every 1 in 5 men will face osteoporotic fractures in their lifespan (Sozen et al., 2017). Osteoporosis affects an estimated 34 million Americans leading to 2 million fractures annually. Osteoporotic fractures are fairly common; almost half of the white women will develop osteoporotic fractures during their lifetimes (Koyama et al., 2013). Despite the development of screening tools and efficacious treatments to lower the fracture risk, there is still a screening and treatment gap that exists in osteoporosis (Nanes & Kallen, 2014).

Bone remodeling is a process that involves the removal of older bone and replaced by a new bone, which is used to repair microfractures thereby assisting in maintaining healthy bone.

Menopause and aging will cause an imbalance between bone formation and resorption (Sozen et al., 2017). After 30 years of age, bone density continues to fall in both sexes, with loss accelerating in women after menopause (Nanes & Kallen, 2014). Therefore, females are at a higher risk of developing osteoporosis. The bone turnover is almost double in menopausal women (Nanes & Kallen, 2014).

Bone density declines with age and by 70 years bone mass will decrease by 30–40 percent (Tella & Gallagher, 2014). The factors that affect bone mass are age, gender, race, genetics, reproductive status, low calcium intake, and exercise (Tella & Gallagher, 2014). There are pharmacological (Alendronate, Ibandronate, and Zoledronic acid, etc.) and non-pharmacological management (exercise, diet, Vitamin D, calcium, smoking, etc.) for osteoporosis. It happens mostly at the hip, vertebra, and wrist. According to NIAMS, we can take steps to prevent osteoporosis and broken bones by doing weight-bearing exercises or lifting weights, eating a well-balanced diet rich in calcium and vitamin D, not drinking too much alcohol, not smoking, and taking the prescribed medications. The study by (Burge et al., 2007), has noted that osteoporosis prevention, treatment, and education efforts should focus on all the sites, not just the hip and vertebra.

Although osteoporosis predisposes to bone fractures, most patients suffering from osteoporosis will not experience fracture until it is evident (Nanes & Kallen, 2014). Several medications and conditions have a secondary effect that leads or predisposes to osteoporosis.

Diagnosis of Osteoporosis

BMD

To act before the bone degrades to a critical level and prevent complications, most clinicians use a bone mineral density (BMD). BMD is a value to understand the number of minerals

per unit area and is expressed in g/cm^2. It helps to determine bone strength (Office of the Surgeon, 2004). BMD is used to measure bone strength, fracture risk, and is used primarily to assess osteoporosis (Wang et al., 2015). BMD score is compared to a healthy individual's average BMD scores.

T-score: osteoporosis, osteopenia, and normal

T-score is measured as the amount that the value differs from the norm. The World Health Organization has categorized into different types based on T-score. T-scores above −1.0 is normal; T-scores between −1.0 and −2.5 is osteopenia; T-scores −2.5 or below are osteoporotic (Ramos, 2016).

DXA

Dual-energy X-ray Absorptiometry (DXA) as shown in Figure 1 is considered as the gold standard and reliable tool to measure BMD. The DXA is widely used because of its various advantages such as low radiation, fast scan time, ease of use, and precision (Lee et al., 2009). It is also inexpensive when compared with other options that measure bone density. The lumbar spine and hip are the most common sites chosen for BMD measurement. Though it is widely used it is limited too. Its inability to quantify bone volume, when the rays are passed the measured attenuation is a combination of soft tissues and bones (Lee et al., 2009), inability to position the subject properly (requires highly skilled or trained individuals), and inability to incorporate structures into readings (Rosen et al., 2013).

In the supine DXA scan of the AP view, the vertebral bodies and posterior elements are merged and cannot differentiate the posterior elements properly. Whereas in lateral DXA it is not merged, and it can be more sensitive to identify the age-related bone loss and thus identifying

osteoporosis. The disadvantage is that it is not accurate because of the inappropriate positioning of the patients and also interference of the iliac spine and ribs (Wang et al., 2015).

Figure1. A DXA machine from Hologic.

The International Society of Clinical Densitometry (ISCD) recommends specific sites to determine osteoporosis (Lewiecki et al., 2008). ISCD recommends measuring BMD at both posterior-anterior (PA) spine and hip in all patients.

Determinants of Bone Strength

Bone mass and bone quality

Bone is composed of collagen and minerals. Mineral accounts for most of the bone mass (Rosen et al., 2013). Bone mass and bone quality are the two components that determine bone strength (*Osteoporosis: cause, treatment, prevention / [prepared by the National Institute of Arthritis and Musculoskeletal and Skin Diseases, National Institutes of Health]*, 1986). Accurate measurement of bone strength is necessary for clinical decision-making regarding osteoporosis (Wang et al., 2015). With early diagnosis, fractures can be avoided, and osteoporosis can be preventable. Osteoporosis does not have many clinical symptoms for the patient to present. It is

sometimes referred to as a silent disease as people do not realize they have porous bones until they face a fracture (Ramos, 2016).

Bone mass is indicative of the amount of bone available. Bone quality includes several parameters, such as micro-architecture, bone turnover, and mineralization (Ramos, 2016).

"The failure load of the vertebral body depends on the density and architecture of the trabecular bone and the shape, size, and organization of the vertebral body"(Myers & Wilson, 1997). The BMD determined by DEXA correlated strongly with the compressive strength. "With aging and osteoporosis, there are compromises in the strength of the trabecular bone and the structural capacity of the vertebral body" (Myers & Wilson, 1997).

Vertebral fracture is the most common, accounting for 27% with the prevalence of around 30-50% among those 50 years above of all osteoporotic fractures. Vertebral fractures have significant morbidities such as reduced pulmonary function, back pain, functional limitations, therefore, affecting the quality of life. So, identifying them is very important and DEXA has been shown as the gold standard to determine BMD (Anderson et al., 2014).

Bone architecture is important in determining the function and strength of Bone. Bone is separated into cortical (compact) and cancellous (trabecular/spongy) bone. Cortical bone is characterized by being resistant against bending and torsion forces and makes up roughly 80% of skeletal mass and is often found surrounding the internal cavity of bones as a protective layer. Trabecular bone makes up roughly 20% of the mass of bones, its architecture is set with high porosity as a way to respond and resist compression forces (Ramos, 2016). With osteoporosis, the loss of trabecular bone mass is considered more damaging to overall structures. The trabecular bone structure undergoes degradation within the vertebral body with the process of aging

(Whitmarsh et al., 2013). The trabecular plates are lost, thus makes the bone architecturally weak with a reduction in mass, and this leads to an increased risk of fracture (Sozen et al., 2017).

Limitations of DXA

Several studies have noted that measurement of BMD alone is not sufficient to estimate the fracture risk (Bolotin & Sievänen, 2001; Dong et al., 2018; Dong, Pinninti, Lowe, et al., 2015; Pinninti, 2015; Wang et al., 2015). The measurement of BMD by DXA only gives a rough estimate of fracture risk (Dong et al., 2013). BMD is defined as the amount of bone mass and it indicates the quantity, however, it does not say about the bone quality. Bone quality includes all features and characteristics such as architecture, bone turnover, mineralization, and damage accumulation that influence bones' ability to resist fractures (Dong et al., 2013). The microarchitecture of trabecular bone is one of the major contributors to bone fragility (Dong et al., 2013).

BMD alone cannot assess the amount of fracture risk (Kazakia & Majumdar, 2006), and also it does not adequately assess the impact of therapeutic interventions (Marshall et al., 1996). The importance of microarchitecture in assessing bone strength has been brought to the attention of the clinical community (Ciarelli et al., 1991). As osteoporosis targets the trabeculae with thinning and structural connectivity loss, it is important to measure it (Kazakia & Majumdar, 2006).

The objective of this Study

Therefore, the objective of this study is to improve the prediction of bone fractures with DXA through not only BMD but also by measuring the microarchitecture parameters of trabecular bone.

Chapter 2

LITERATURE REVIEW

Three-dimensional Imaging Modalities for Assessing Bone Microarchitecture

Imaging technologies have the ability to evaluate bone micro-architecture so thus helps in assessing osteoporotic status. An advantage of using 3D imaging techniques is that they help in distinguishing trabecular bone from the cortical bone (Ramos, 2016). The use of them in both clinical studies and research is growing.

Quantitative ultrasound (QUS)

Quantitative ultrasound (QUS) has been introduced recently for evaluating bone density in the appendicular skeleton. The advantage of using QUS is that it involves no radiation, a portal device, is inexpensive and scans can be quickly executed (Kazakia & Majumdar, 2006). The primary disadvantage of it is that it lacks sensitivity (Moyad, 2003), making QUS inappropriate for long-term monitoring of osteoporosis or monitoring the response to drug therapy. Currently, it's used as a screening tool, with confirmation of diagnosis via DXA evaluation (Kazakia & Majumdar, 2006).

Quantitative computed tomography (QCT)

Quantitative computed tomography (QCT) was first developed for the assessment of the spine but now it can be applied to the hip and appendicular skeleton (Ramos, 2016). The advantage of QCT over DEXA is that it evaluates three-dimensional spatial resolution, thus this provides the assessment to volumetric BMD and microarchitecture. QCT also allows examination of the separate contributions of cortical and trabecular bone (Kazakia & Majumdar, 2006; Ramos, 2016). “QCT images can be separated into different types of tissue, such as lean and adipose, as well as a cortical and cancellous bone” (Lee et al., 2009). Limitations of QCT include a higher radiation

dose than DXA, greater expense, and limited availability of equipment (Kazakia & Majumdar, 2006; Ramos, 2016). “Standard CT machines can be transformed into QCT machines by using a mineral equivalent phantom spine to calibrate the image” (Bouxsein, 2003).

High-resolution peripheral quantitative computed tomography (HR-pQCT)

The primary tools for measuring volumetric density and bone structure are QCT and are now advanced with high-resolution peripheral quantitative computed tomography (HR-pQCT). It is effective in determining the microarchitecture of trabecular bone both in vivo and in vitro (Dong et al., 2013; Ramos, 2016).HR-pQCT is restricted to peripheral sites such as the distal radius and distal tibia. “HR-pQCT scanners still exist in research environments but their use has dramatically increased since their introduction in 2005” (Nishiyama & Shane, 2013)). Currently, the number of devices available and the lack of standardization limit the widespread clinical use of HR-pQCT (Bouxsein, 2003; Kazakia & Majumdar, 2006; Nishiyama & Shane, 2013).

At the highest end of the resolution, hierarchy resides in micro-computed tomography (μCT). μCT can be used to visualize fine trabecular structure (Kazakia & Majumdar, 2006). It is now limited to imaging biopsies and small animals and radiation is too high for human use.

Magnetic Resonance Imaging (MRI)

High-resolution MR bone imaging is most often performed at peripheral sites such as the heel, knee, and wrist and helps indirectly assessing the structure of bone (Gokalp et al., 2011). “High-resolution MRI is referred to as a direct method for two-dimensional or three-dimensional imaging of trabecular bone networks” (Koyama et al., 2013; Ramos, 2016). With the recent development of surface coils and new pulse sequences, high-resolution imaging of the proximal femur has been accomplished (Krug et al., 2005).

Magnetic resonance imaging (MRI) has sufficient spatial resolution and high-contrast resolution and is used in the diagnosis of lumbar vertebra diseases (Ramos, 2016). The trabecular properties from MRI have been shown to have a close correlation with other measurements of trabeculae from other high-resolution imaging techniques, like that of HR-pQCT (Dong, Pinninti, Lowe, et al., 2015; Dong, Pinninti, Tvinnereim, et al., 2015; Pinninti, 2015). The advantage of MR imaging is the lack of ionizing radiation exposure (Kazakia & Majumdar, 2006; Oei et al., 2016). A limitation in clinical MR imaging is the long acquisition time required, taking the scans difficult, uncomfortable for certain patients, more costly, and also produces a lower spatial resolution than CT. (Dong et al., 2013; Kazakia & Majumdar, 2006; Oei et al., 2016).

The bone strength is dependent on its architecture, so MRI and CT can produce high-resolution images that can give us information about the 3D structure. High-resolution peripheral quantitative computed tomography (HR-pQCT) is one of the important 3D imaging techniques. The studies have shown its importance in both clinics and in vitro situations, they are effective in assessing the microarchitecture in trabecular bone but because of its limited access and affordability, it can't be used by the public population (Dong et al., 2013).

Some new techniques have been introduced to enhance the prediction of bone fractures from DXA images; fractal texture analysis, topological analysis, finite element analysis, trabecular bone score based on experimental variogram (Dong, Pinninti, Tvinnereim, et al., 2015).

Two-dimensional Imaging Modalities for Assessing Bone Fragility

Hip structure analysis

Hip structure analysis is "is a way that uses the properties of dual-energy x-ray absorptiometry (DXA) images to derive geometric parameters for the hip that are related with bone

strength" (Ackerman et al., 2013). This is a validated technique used to assess hip bone geometry and avoids the significant radiation associated with other imaging modalities. To do hip structure analysis, some factors should be obtained from DXA scan at the hip that includes-a cross-sectional moment of inertia, the section modulus, the buckling ratio, and the cortical thickness (Bonnick, 2012; Dong, Pinninti, Lowe, et al., 2015; Dong, Pinninti, Tvinnereim, et al., 2015).

Fractional risk assessment tool (FRAX)

The fractional risk assessment tool (FRAX) is the most widely used fracture prediction program worldwide (Kanis et al., 2017). The FRAX assessment tool has been shown to have success when predicting long-term fracture risk (Ramos, 2016). However, the overlap between the risk of fracture and fracture occurrence has been noted to be a significant limitation (WHO, 2004).

Fractal analysis

The fractal analysis is used to find geometric and microstructural features of bone from 2D projection image modalities through imaging process techniques. Fractal analysis has been used on high-resolution 2D radiography images in both clinical and in vitro studies (Dong et al., 2013). It is used to identify the correlations between fractal dimension and microarchitectural features of trabecular bone in high resolution. However, it does not find 2D projection images with moderate resolution. It requires large projection surfaces, as DXA images use smaller areas with a lower resolution it is not suitable for fractal analysis (Ramos, 2016).

Trabecular bone score (TBS)

The trabecular bone score is widely used in the assessment of fracture risk (Dong, Pinninti, Lowe, et al., 2015; Silva et al., 2014). It is a textural parameter that uses greyscale images from DXA to compute the micro-architecture of bones. "TBS is related to bone microarchitecture and provides skeletal information that is not captured from the standard bone mineral density (BMD)

measurement" (Silva et al., 2014). The higher and lower TBS values correlate with the skeletal microstructure, The higher the value the better the skeletal microstructure and vice versa (Silva et al., 2014). "TBS is a textural index that evaluates pixel gray-level variations within the lumbar spine DXA image, providing an indirect index of trabecular microarchitecture" (Silva et al., 2014). "A dense trabecular microstructure projected onto a plane generates an image containing a large number of pixel value variations of small amplitude. Conversely, a 2D projection of a porous trabecular structure produces an image with a low number of pixel value variations of high amplitude" (Silva et al., 2014). "TBS is determined by a computed variogram of the image of the region of interest from the DXA scan. This is calculated as the sum of the squared gray-level differences between pixels at a specific distance. The TBS value is calculated as the slope of the log-log transform of the variogram" (Silva et al., 2014). However, TBS values should not entirely be used to determine treatment recommendations nor be used for monitoring 13 bisphosphate treatment in postmenopausal women with osteoporosis (Rosen, 2013).

Stochastic predictors for experimental variogram

The study done by Dong et al., 2015 has demonstrated the stochastic assessment of bone mineral distribution from DXA images when combined with BMD measurements can serve as an important tool in enhancing the prediction of osteoporosis for postmenopausal women.

By using stochastic predictors derived from the DXA images, the variation of the bone mineral density can give a better assessment of the different areas of the bone (Ramos, 2016). The study done by Dong et al., 2013, has proposed a stochastic method to examine 2D images of trabecular bone and assess the variance of BMD distribution.

Stochastic parameters represent the spatial variation within the 2D image (Ramos, 2016). Presently, the use of descriptive statistic values, like mean and standard deviation, describes the

heterogeneity of bone but does not mention the spatial qualities of bone (Dong et al., 2013; Ramos, 2016). The studies have shown that the stochastic predictors from the DXA images have a significant correlation with the strength and microarchitecture of trabecular bone (Dong, Pinninti, Tvinnereim, et al., 2015).

The variogram is a descriptive statistic that explains the spatial variation over different areas of bone. Here it represents BMD distribution from the DXA scans. Spatial variation of BMD map from DXA scans are denoted in two variables- one is semi variance γ(h) which is defined as half of the expected squared differences between any paired data values (Dong, Pinninti, Lowe, et al., 2015), and another one is lag (h) (Dong et al., 2013). These are expressed using variograms.

$\gamma(h) = \frac{1}{2} E[\{z(x)-z(x+h)\}]^2$

z is a random function of the bone property that varies continuously in space, x denotes the spatial coordinates of locations, and h, also known as lag, is a vector representing the Euclidean distance and direction between any two data locations (Dong et al., 2013).

The experimental variogram for the BMD map of vertebrae is computed as an average of semi-variance values at different locations that have the same value of lag.

$$\gamma(h) = \frac{1}{2m(h)} \sum_{i-1}^{m(h)} \{z(x_i) - z(x_i + h)\}^2$$

here m(h) is the number of data pairs $\{z(xi), z(xi + h)\}$ for observations separated by" h."

Correlation length describes the degree of smoothness or roughness in the BMD map (Dong et al., 2013). A relatively large correlation length implies a smooth variation, whereas a small correlation length corresponds to rapid variations of the bone mineral density over the spatial domain. The sill variance of the variogram is representative of the variance within the BMD map. The sill variance is defined as the limit of the experimental variogram tending to infinity lag

distances (Ramos, 2016). It can be referred to as the "amplitude" or “maximum value” of a certain component of the semi-variogram (Ramos, 2016).

The study done by Dong et al., 2015 has found significant correlations between stochastic predictors and microarchitecture parameters. They also found that the sill variance, representing SD of the BMD map to some extent, has a positive correlation with bone volume, trabecular thickness, trabecular number, and connectivity density. Another study by (Dong et al., 2018) has demonstrated that the stochastic predictors from the simulated DXA scans are positively correlated with vertebral strength.

Posterior elements on BMD measurement

As we discussed earlier, the vertebral fracture prevalence is rapidly increasing with aging and reaching as high as 50% among women older than 80 years (Wang et al., 2015). So, it is very important to measure the spine when diagnosing osteoporosis. The posterior elements contribute little to the compressive strength of the spine (Bjarnason et al., 2005). There is controversy over whether to include the posterior elements of the spine or not. The study by Wang et al., 2015 has mentioned the importance of posterior elements and their contribution to BMC (Bone Mineral Content). They concluded that posterior elements are the primary contributor to vertebral BMC and BMD measurements. Furthermore, the studies done by Lee et al., 2009 have used QCT to measure the impact of posterior elements in DXA AP spine measures. They concluded by saying that the posterior elements have contributed a significant amount in BMC, there is a difference that exists between males and females, and the contribution of posterior elements is steady in young subjects after puberty.

Purpose of this Study

The purpose of this study is to examine the relationship between stochastic predictors of simulated DXA images with the microarchitecture of trabecular bone. This study also involves the stochastic assessment of 2D images which are generated from 3D CT images of a human vertebra with and without posterior elements.

SPECIFIC AIMS AND EXPECTED OUTCOMES

Overall, the objective of this study is to find out whether the removal of posterior elements will improve the correlation between stochastic predictors and the microarchitecture of trabecular bone. To do so, we will have three specific aims:

Aim 1: To identify the correlations between stochastic predictors and microarchitecture parameters for simulated DXA images with intact posterior elements.

We expected significant correlations between stochastic predictors and microarchitecture parameters for simulated DXA images with intact posterior elements.

Aim 2: Identify the correlations between stochastic predictors and microarchitecture parameters for simulated DXA images without posterior elements.

We also expected that significant correlations will be observed between stochastic predictors and microarchitecture parameters for simulated DXA images without posterior elements.

Aim 3: Compare these correlations from specific aims 1 and 2 and find out whether removal of posterior elements will improve the correlation between microarchitecture of trabecular bone and stochastic predictors from simulated DXA images.

We anticipated that the correlations between microarchitecture parameters of trabecular bone and stochastic predictors will be significantly higher in simulated DXA images without posterior elements than those with posterior elements.

Chapter 3

EXPERIMENTAL DESIGN AND METHODS

Overview of study design

MicroCT images of human lumbar vertebrae were obtained from tissue donors. Then, the MicroCT images were imported into *Microview* to measure microarchitecture parameters. Additionally, simulated DXA images with and without posterior elements were generated from 3D MicroCT images of human lumbar vertebrae. Stochastic parameters such as correlation length (L), and sill variance (C) were calculated by fitting a theoretical model onto the experimental variogram of simulated DXA images with and without posterior elements. Finally, the influence of posterior elements on the relationship between microarchitecture trabecular bone and stochastic predictors were determined.

Subjects and specimen preparation

The study included human lumbar vertebrae (N=18) from five tissue donors (4 males and 1 female). MicroCT scans of human lumbar vertebrae were performed at The University of Texas Health Science Center at Tyler (UTHSC). Before scanning, soft tissue was removed over the cadaver's spine and all lumbar vertebrae were dissected out of it. The posterior elements were intact and remained with the human vertebrae. Any bone disease (i.e., bone metastasis, Paget's disease of the bone, major osteoarthritis) or fracture was assessed using DXA. The vertebral specimens were wrapped with gauze and stored at -25°C until Micro-CT image acquisition was performed. A micro-CT scan was performed by following established procedures with an isotropic voxel size of 92 µm. This is the smallest available voxel size in this scanning system for the size of vertebrae used in this study.

3D Micro CT images of human vertebrae

The major application of Micro-CT is to scan a small specimen and generate high-resolution 3D images. Small specimens may include human vertebrae separated from cadavers' spines. Three-dimensional (3D) microarchitecture of bone can also be described using Micro-CT images. Due to its high resolution, Micro-CT can obtain precise 3D images at the micro-level of trabecular bone structure. Although the high resolution is achievable using Micro-CT, scanning large specimens such as a whole vertebral body may require the use of spatial resolution corresponding to a voxel size greater than 100 µm. Because 100 µm is in the order of typical trabecular thickness, partial volume effects will cause errors when computing the stereological parameters for trabecular bone. The Micro-CT machine has its major applications in research areas only, because of its high radiation. Using Micro-CT, the specimen can be scanned at one voxel size, and the raw data reconstructed at a different voxel size. A voxel is defined as a volumetric pixel of the object in a 3D image similar to a pixel of an object in a 2D image.

Simulated DXA images

The present study involved simulated DXA images from 3D Micro CT scans. This study involved the use of the *ImageJ application* for simulation and separation of the human vertebrae into vertebrae body and posterior elements. The following are the steps involved-

- The stitched image was opened using the plugin *Input-Output* with the option *Multi VFF Opener*. The stitched image consists of three volumes scanned in various regions of the whole vertebra.
- Converted stack of 16-bit images to stack of 8-bit images. A median filter with a radius of two pixels was used to remove the noise in a stack of grayscale images.

- The stack of threshold images was obtained by adjusting the threshold value with a *threshold* option. Tube and phantom were removed from threshold images.
- The vertebral body was separated from posterior elements (Figures 2 and 3). Threshold images were purified using the plugin *Bone* with an option to *purify*.
- After purification saved all the stack of images of the vertebral body in a separate folder to convert the format of images.
- Imported the stack of threshold images (vertebral body) into *Microview* to measure microarchitecture parameters.
- Cylindrical region of interest (ROI) was used to measure microarchitecture parameters of the vertebral body using *Bone analysis.* The maximum volume of the vertebral body is covered without a cortical shell using cylindrical ROI.

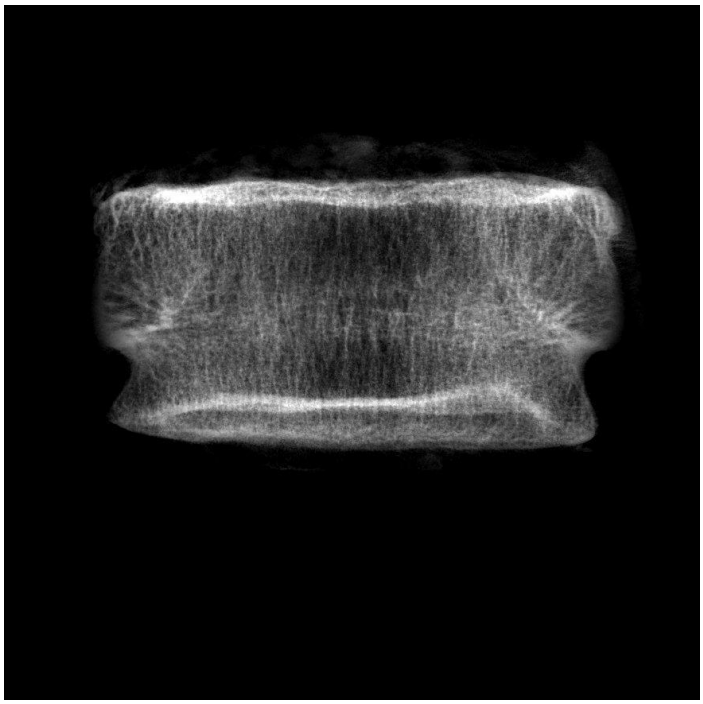

- Figure 2. Simulated DXA image including only the vertebral body, not the posterior elements.

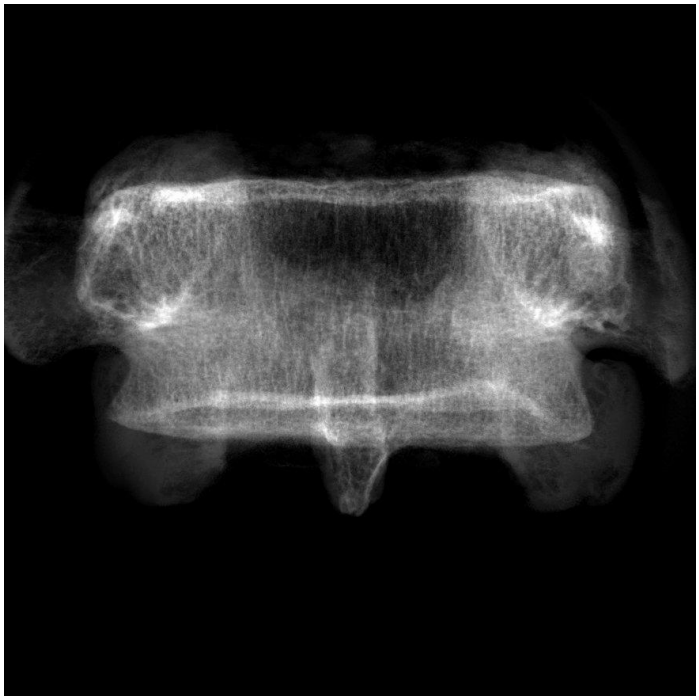

- Figure 3. Simulated DXA image showing both vertebrae body and posterior elements.

Measuring microarchitecture parameters of trabecular bone

Bones are commonly imaged using computed tomographic (CT) and X-ray micro-computed tomographic (μCT) systems for research purposes, such as investigating trabecular and cortical changes in osteoporosis. Many of the scans were over 1GB, and the existing software could not process large datasets, required a per-machine launch fee, or did not implement the required features. We needed to open varied image formats from diverse instruments, then pre-process, analyze and visualize scans efficiently on several different computers, remote from scanning hardware. We took advantage of the existing functionality and flexible plugin architecture of the public domain image-processing program *ImageJ* (Figure 4). The images are imported into micro view to calculate the microarchitecture parameters of lumbar vertebrae (Pinninti, 2015).

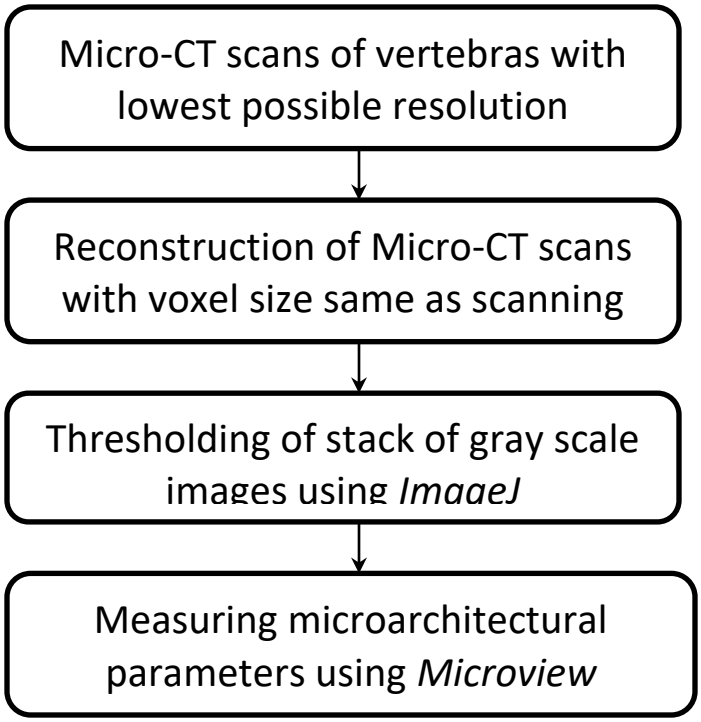

Figure 4. The sequence of steps to evaluate microarchitecture parameters of specimens

Experimental Variograms and Stochastic Predictors

The variograms used stochastic predictors to describe the distribution of BMD in simulated DXA images. This distribution talks about the correlation with the microarchitecture of bone. The variogram is expressed in two values: semi-variance and lag. An exponential variogram model was fitted over the BMD map for the simulated DXA scans. Code was developed in MATLAB (Mathworks, Natick, MA, USA) software to obtain the BMD map. The Micro CT images were imported, and the file was opened using MATLAB. Then MATLAB was run to find the variograms.

After completion, the MATLAB program was showing the constructed area of interest, a histogram of the z-values, the sill, lag, and nugget values, as well as the exponential model over the variogram.

Stochastic assessment of BMD map from simulated DXA scans

Stochastic assessment of inhomogeneity or BMD distribution from simulated DXA images can be described by experimental variograms, which are widely used in geosciences (Atkinson & Lloyd, 2007). In this study, the spatial variation of the BMD map from DXA scans was evaluated using a variogram, which could be expressed in two parameters: semi-variance and lag. Current techniques for quantifying bone heterogeneity consist of descriptive statistics such as mean and standard deviation. However, these parameters do not describe the spatial variations of bone properties. The stochastic method allows us to assess the quality of bone.

The semi-variance $\gamma(\mathbf{h})$ will be defined as half of the expected squared difference between any paired data values $\{z(\mathbf{x}), z(\mathbf{x}+\mathbf{h})\}$:

$$\gamma(h) = \frac{1}{2} E[\{z(x) - z(x+h)\}]^2$$

where **z** is a random function of the indentation modulus of bone that varies continuously in space, **x** denotes the spatial coordinates of locations, and **h**, also known as lag, is a vector representing the Euclidean distance and direction between any two data locations.

The experimental variogram for the BMD map of vertebrae will be computed as an average of semi-variance values at different locations that have the same value of lag:

$$\overset{\Lambda}{\gamma}(h) = \frac{1}{2m(h)} \sum_{i-1}^{m(h)} \{z(x_i) - \mathrm{z}(\mathrm{x}_i + h)\}^2$$

Where *m(h)* is the number of data pairs $\{z(x_i), \mathrm{z}(\mathrm{x}_i + h)\}$ for observations separated by h.

A hole-effect theoretical variogram model will be fitted over the experimental variogram of the BMD map obtained from DXA scans. The main reason for using the hole-effect model is that the experimental variogram of the BMD map decreased from its maximum to a local minimum and then increased again, indicating fairly regular repetition in the process.

The mathematical definition of the hole effect model is given as

$$\gamma(h) = c(1 - \frac{\sin(\mathrm{h}\,\pi / \mathrm{L})}{(\mathrm{h}\,\pi / L)})$$

where $\gamma(\mathrm{h})$ is the semi-variance as a function of lag (h), '*L'* is referred to as the correlation length, and '*c*'s is referred to as sill variance of BMD map.

Figure 5 is an example of an experimental variogram and stochastic predictors from simulated DXA images of human vertebrae without posterior elements.

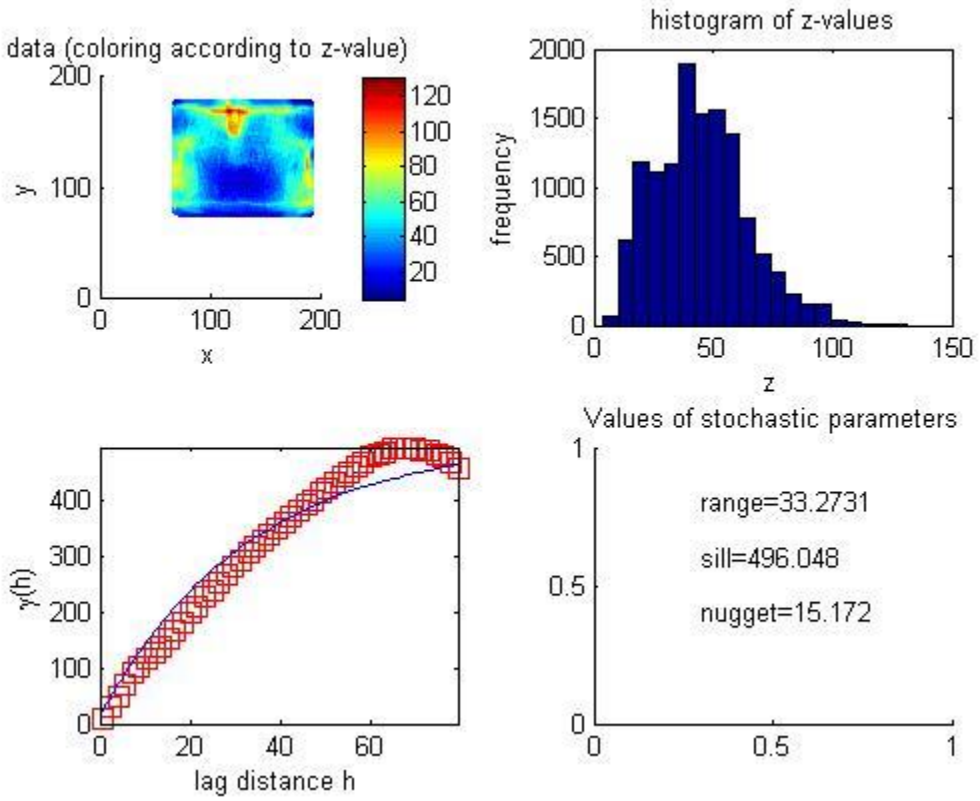

Figure 5. Experimental variogram and stochastic predictors of a human vertebra without posterior elements.

Statistical analysis

We used SPSS to perform linear regression to evaluate the relationship between microarchitecture parameters of trabecular bone and stochastic predictors from simulated DXA images. We then compared the correlation coefficients from these analyses between simulated DXA images with and without posterior elements. Then, the effects of posterior elements on the stochastic predictors of the human lumbar spine were determined.

Chapter 4

Results

In this study, eighteen lumbar vertebrae, including L1 (N=4), L2 (N=4), L3 (N=4), L4 (N=4), and L5 (N=2), were used. Among these 18 vertebras, experimental variograms of three vertebrae images were not produced due to memory problems. DXA, stochastic, and microarchitecture parameters of all the vertebrae and correlation analysis of these parameters were provided in this chapter.

Microarchitecture parameters calculated from micro-CT images

Microarchitecture parameters such as BV/TV, BS/BV (mm^2/mm^3), Tb.Th (mm), Tb.N (1/mm), Tb.Sp (mm), and Conn. Dn (mm^{-3}) were calculated from Micro-CT images of each vertebral body (Table 1).

Table 1. Microarchitecture parameters of lumbar vertebral bodies

No	Specimen	BV/TV	BS/BV	Tb.Th	Tb.N	Tb.Sp	Conn.Dn
1	69099-L1	0.285078	8.167961	0.244859	1.149912	0.621719	1.29605
2	69099-L2	0.271276	8.533917	0.234359	1.157523	0.629555	1.33995
3	69099-L3	0.250239	8.906055	0.224566	1.114323	0.67284	1.2631
4	69099-L4	0.239621	8.734281	0.228983	1.046458	0.726622	1.08152
5	69099-L5	0.237176	8.761235	0.228278	1.038979	0.734205	1.14732
6	69111-L1	0.188431	9.276805	0.215591	0.874021	0.928546	0.77694
7	69111-L2	0.166298	9.765169	0.20481	0.811963	1.026773	0.7262
8	69111-L3	0.146029	10.03701	0.199263	0.732846	1.16528	0.58238
9	69111-L4	0.152348	9.675566	0.206706	0.737028	1.150094	0.63762
10	69111-L5	0.186262	9.042307	0.221182	0.842119	0.966298	0.79322
11	69013-L4	0.180221	8.95426	0.223357	0.806872	1.015997	0.63467
12	01595-L1	0.243544	8.071331	0.247791	0.982863	0.769645	0.93442
13	01595-L2	0.280634	7.414707	0.269734	1.04041	0.691425	1.00038
14	01595-L3	0.253995	7.741705	0.258341	0.983176	0.758771	0.87413
15	01854-L1	0.226677	8.602905	0.23248	0.975042	0.793117	1.02925
16	01854-L2	0.23002	7.840973	0.25507	0.90179	0.853835	0.85709
17	01854-L3	0.174049	10.00913	0.199817	0.87104	0.948236	0.78386

18	01854-L4	0.174745	9.886659	0.202293	0.863823	0.955351	0.82901

BV/TV- bone volume fraction, *BS/BV*- bone surface to volume ratio, *Tb.Th*- trabecular thickness, *Tb. N*- trabecular number, *Tb.Sp*- trabecular separation, *Conn.Dn*- connectivity density, *BMC*-bone mineral content, *BMD*-bone mineral density

Stochastic parameters of vertebrae with and without posterior elements

The stochastic parameters (range, sill, and nuggets) of the 15 vertebrae with and without posterior elements were described in Table 2. The descriptive statistics of stochastic parameters from simulated DXA and microarchitecture parameters from MicroCT images were summarized in Table 3.

Table 2. Stochastic parameters of vertebrae body and whole vertebrae.

No.	Specimen	Range (vertebrae body)	Sill	Nugget	Range (Whole Vertebrae)	Sill	Nugget
1	69099-L1	68.2353	134.3401	30.4939	37.7683	520.2461	27.6219
2	69099-L2	53.8953	186.8241	31.3182	33.8325	506.47	26.7275
3	69099-L3	49.8181	186.2645	17.2568	36.3272	644.694	19.5062
4	69099-L4	46.1162	91.1307	7.9287	24.1024	314.1163	2.97E-07
5	69099-L5	-	-	-	-	-	-
6	69111-L1	50.6538	105.8393	15.4043	24.8181	333.4896	1.39E-08
7	69111-L2	48.8308	132.1677	39.2475	24.4203	385.0225	7.8936
8	69111-L3	56.1711	170.6184	17.3762	36.6599	512.7395	22.8674
9	69111-L4	62.927	145.1359	19.7392	42.3221	261.5817	22.8046
10	69111-L5	-	-	-	-	-	-
11	69013-L4	-	-	-	-	-	-
12	01595-L1	61.1754	117.8738	29.205	28.7504	344.0757	17.5824
13	01595-L2	43.4211	98.2988	31.5507	33.2731	496.048	15.172
14	01595-L3	44.9722	106.4493	12.5682	27.9058	414.4187	9.8245
15	01854-L1	22.4892	152.0043	26.9114	18.2945	416.1947	6.6623
16	01854-L2	23.9821	174.2858	18.2541	31.6667	729.3398	23.1514

17	01854-L3	22.9349	171.7619	16.2548	32.9932	644.6091	24.1279
18	01854-L4	28.7555	260.1758	3.4911	23.2081	464.3458	3.5788

Table 3. Descriptive statistics of microarchitecture parameters and stochastic parameters

Parameter	**Mean ± SD**	**Range**
BV/TV	0.215±0.045	0.146-0.285
BS/BV (mm^2/mm^3)	8.856±0.809	7.414-10.03
Tb.Th (mm)	0.227±0.021	0.199-0.269
Tb.N (1/mm)	0.940±0.133	0.732-1.157
Tb.Sp (mm)	0.856±0.170	0.621-1.165
Conn.Dn (mm^{-3})	0.921±0.231	0.582-1.339
Range (Vertebral body) (mm)	45.625±14.865	22.489-68.235
Sill$(g/cm^2)^2$	148.878±44.631	91.130-260.175
Nugget$(g/cm^2)^2$	21.133±9.933	3.491-39.247
Range (whole vertebrae)	30.422±6.616	18.294-42.322
Sill	465.826±133.585	261.581-729.339
Nugget	15.168±9.722	.00000001-27.621

Pearson correlation coefficient analysis of stochastic predictors and microarchitecture parameters for simulated DXA images

Microarchitecture parameters of trabecular bone from vertebral bodies were correlated with each other (Table 4).

Table 4. Pearson correlation coefficients of microarchitecture parameters

	BV/TV	BS/BV	Tb.Th	Tb.N	Tb.Sp	Conn.Dn
BV/TV	1	–0.862**	0.845**	0.936**	–0.966**	0.858**
BS/BV	–0.862**	1	–0.996**	–0.637**	0.735**	–0.510**
Tb. Th	0.845**	–0.996**	1	0.608**	–0.709**	0.472*
Tb. N	0.936**	–0.637**	0.608**	1	–0.984**	0.972**
Tb. Sp	–0.966**	0.735**	–0.709**	–0.984**	1	–0.930**
Conn.Dn	0.858**	–0.510**	0.472*	0.972**	–0.930**	1

Table 5 showed that the sill variance of simulated DXA images without posterior elements was positively correlated with the bone surface-to-volume ratio (r=0.459), trabecular separation (0.209), and negatively correlated with bone volume fraction (-0.308), trabecular thickness (-0.456), trabecular number (-0.144). Table 6 indicated that the sill variance of simulated DXA images of whole vertebrae is positively correlated with bone volume fraction (r=0.205), trabecular thickness (r=0.141), trabecular number (0.225), and connectivity density (r=0.247) and negatively correlated with the bone surface to volume ratio (r=-0.123).

Table 5 showed that the range of simulated DXA images without posterior elements was positively correlated with bone volume fraction (r=0.141), trabecular thickness (r=0.040), trabecular number (r=0.146), connectivity density (r=0.149), and negatively correlated with the bone surface to volume ratio (r=-0.056), trabecular separation (r=-0.052). Table 6 demonstrated that the range of simulated DXA images of whole vertebrae was minimally correlated with bone volume fraction, the bone surface to volume ratio, trabecular number, trabecular separation, connectivity density.

Table 5 indicated that the nugget simulated DXA images without posterior elements was positively correlated with bone volume fraction (r=0.287), trabecular thickness (r=0.274), trabecular number (r=0.222), connectivity density (r= 0.238), and negatively correlated with bone surface to volume ratio (r=-0.275), and trabecular separation (r=-0.208). Table 6 showed that the nugget of simulated DXA images of whole vertebrae had a mild positive correlation with bone volume fraction (r=0.159), trabecular thickness (r=0.106), trabecular number (r=0.139), connectivity density (r=0.192) and negatively correlated with a bone surface to volume ratio (r=-0.094), trabecular separation (r=-0.066).

Table 5. Pearson correlation coefficients between microarchitectures and stochastic parameters of the vertebral body.

	Range	**Sill**	**Nugget**
BV/TV	0.141	-0.308	0.287
BS/BV	-0.056	0.459	-0.275
Tb.Th	0.040	-0.456	0.274
Tb.N	0.146	-0.144	0.222
Tb.Sp	-0.052	0.209	-0.208
Conn.Dn	0.149	.000	0.238
Range	1	-0.361	0.331
Sill	-0.361	1	-0.291
Nugget	0.331	-0.291	1

$*p \leq 0.05$; $**p < 0.01$; $***p < 0.001$

Table 6. Pearson correlation coefficients between microarchitectures and stochastic parameters of the whole vertebrae.

	Range	**Sill**	**Nugget**
BV/TV	.029	0.205	0.159
BS/BV	0.019	-0.123	-0.094
Tb.Th	-0.001	0.141	0.106
Tb.N	0.006	0.225	0.139
Tb.Sp	0.088	-0.226	-0.066
Conn.Dn	0.043	0.247	0.192
Range	1	0.280	0.832**
Sill	0.280	1	0.536*
Nugget	0.832**	0.536*	1

*$p \leq 0.05$; ** $p < 0.01$; ***$p < 0.001$

Table 7 showed that the correlations between the sill variance and microarchitecture parameters were mostly greater in the vertebral body without posterior elements than the whole vertebrae with intact posterior elements.

Table 7- Pearson correlation coefficients and p-value between microarchitectures and stochastic parameters of the vertebral body and whole vertebrae

	The sill of the vertebral body	**The sill of whole vertebrae**
BV/TV—Pearson correlation	-0.308	0.205

p-value	0.265	0.463
BS/BV—Pearson correlation	0.459	-0.123
p-value	0.085	0.661
Tb.Th—Pearson correlation	-0.456	0.141
p-value	0.87	0.616
Tb.N—Pearson correlation	-0.144	0.225
p-value	0.609	0.421
Tb.Sp—Pearson correlation	0.209	-0.226
p-value	0.454	0.419
Conn.Dn- Pearson correlation	.000	0.247
p-value	1	0.375

Linear regression analysis of microarchitecture parameters of trabecular bone and stochastic predictors from simulated DXA images.

Equations of best fit line with slope and y-intercept as well as coefficient of determination (R^2) were obtained for each linear regression analysis and specified in each Figure. Results of linear regression analysis of microarchitecture parameters of trabecular bone and stochastic predictors from simulated DXA images were described below.

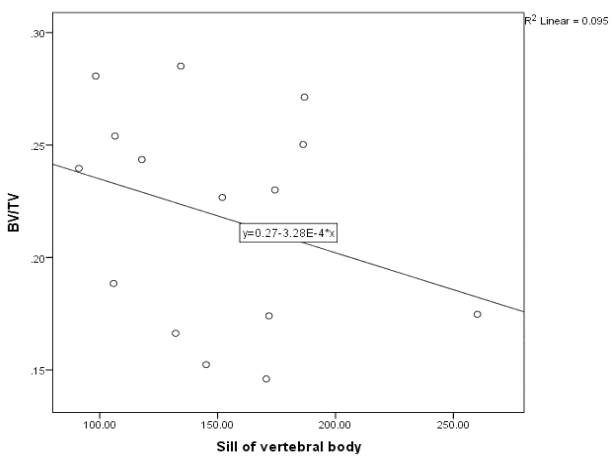
R² Linear = 0.095
BV/TV
y=0.27-3.28E-4*x
Sill of vertebral body

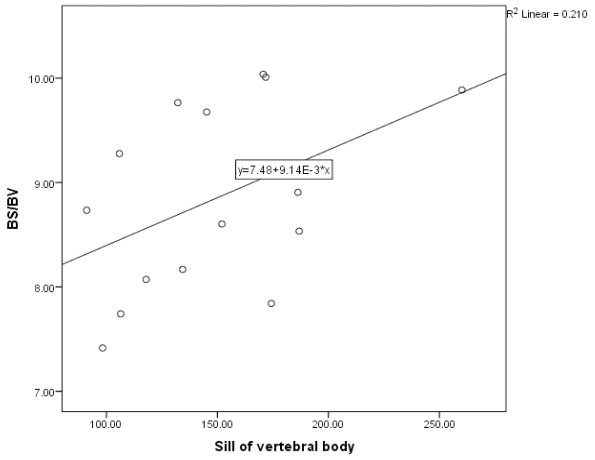
R² Linear = 0.210
BS/BV
y=7.48+9.14E-3*x
Sill of vertebral body

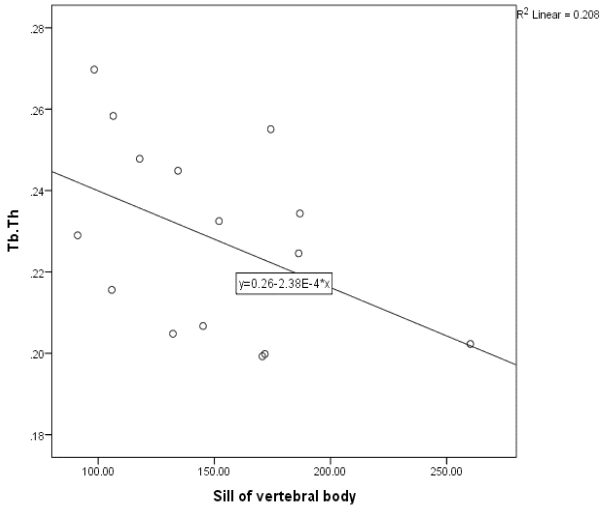
R² Linear = 0.208
Tb.Th
y=0.26-2.38E-4*x
Sill of vertebral body

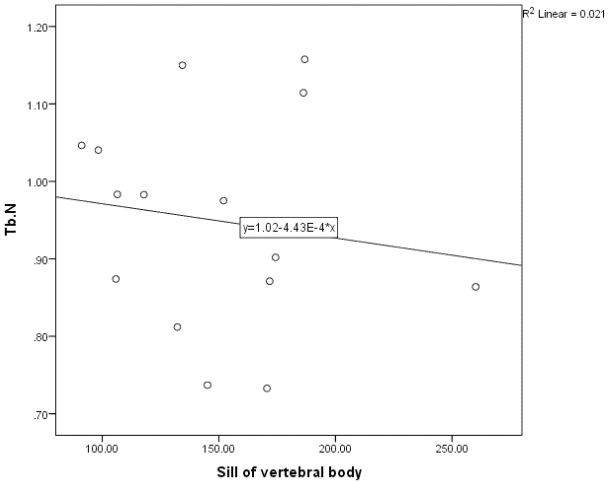
R² Linear = 0.021
Tb.N
y=1.02-4.43E-4*x
Sill of vertebral body

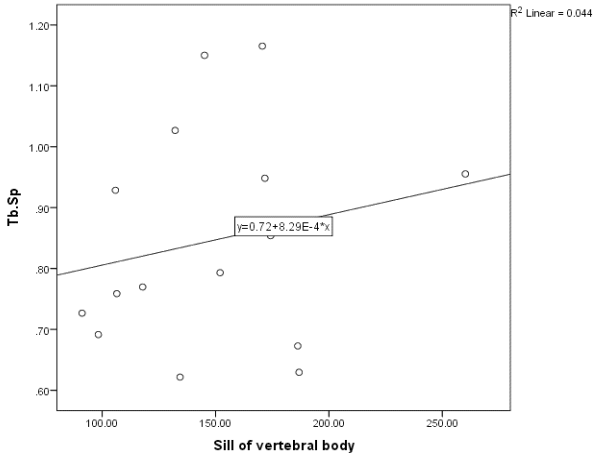
R² Linear = 0.044
Tb.Sp
y=0.72+8.29E-4*x
Sill of vertebral body

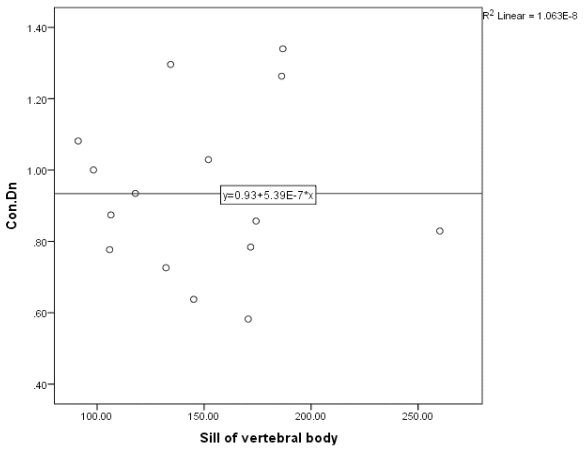
R² Linear = 1.063E-8
Con.Dn
y=0.93+5.39E-7*x
Sill of vertebral body

Figure 6. Linear regression analysis of sill variance of vertebrae without posterior elements and bone volume fraction, the bone surface to volume ratio, trabecular thickness, trabecular number, trabecular separation, and connectivity density.

Sill variance of the vertebral body was negatively correlated with the bone volume fraction, trabecular thickness, and trabecular number. It was positively correlated with the bone surface to volume ratio, Trabecular separation and was not correlated with the connectivity density.

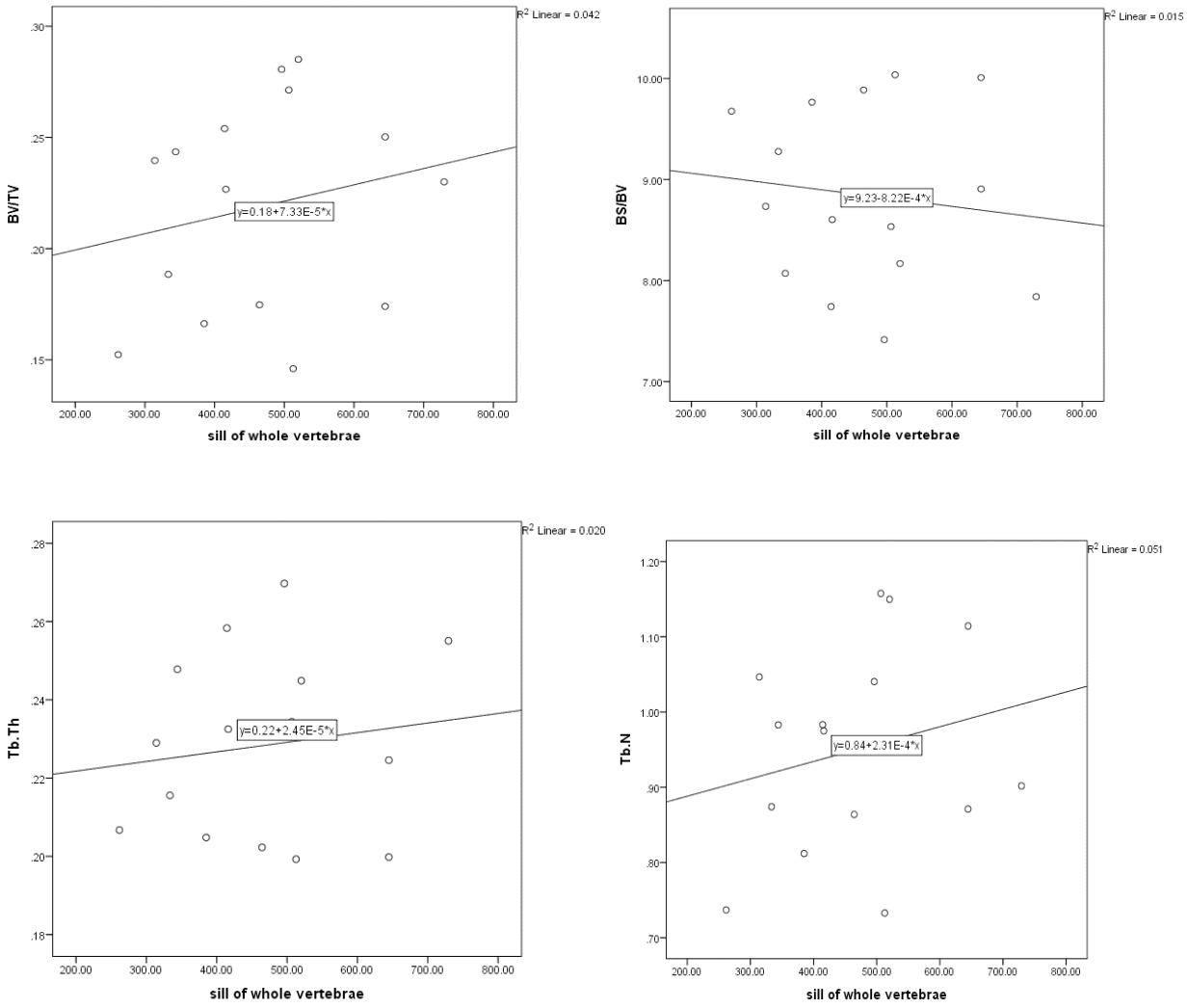

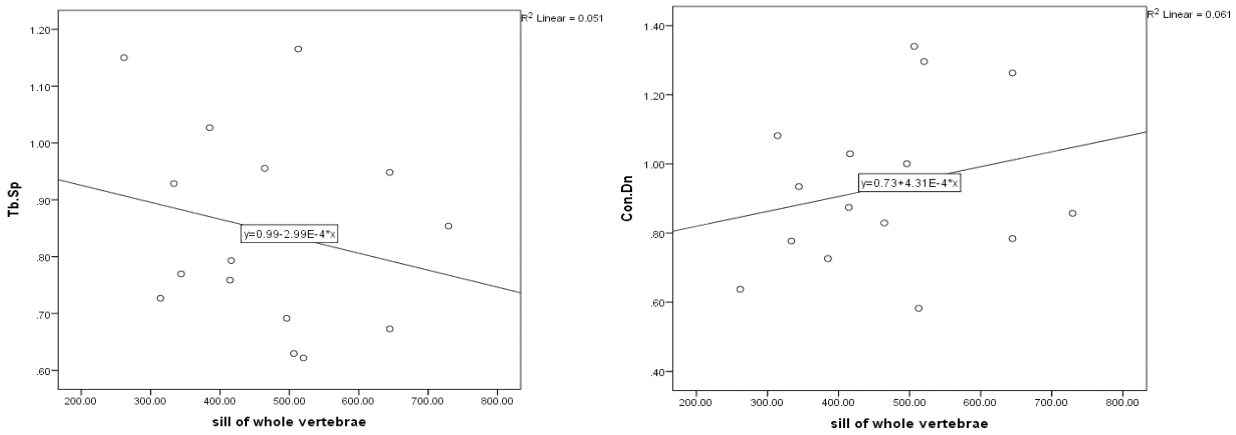

Figure 7. Linear regression analysis of sill variance of whole vertebrae and bone volume fraction bone surface to volume ratio, trabecular thickness, trabecular number, trabecular separation, and connectivity density.

Sill variance of whole vertebrae was positively correlated with the bone volume fraction, trabecular thickness, trabecular number, and connectivity density. It was negatively correlated with the bone surface-to-volume ratio and trabecular separation.

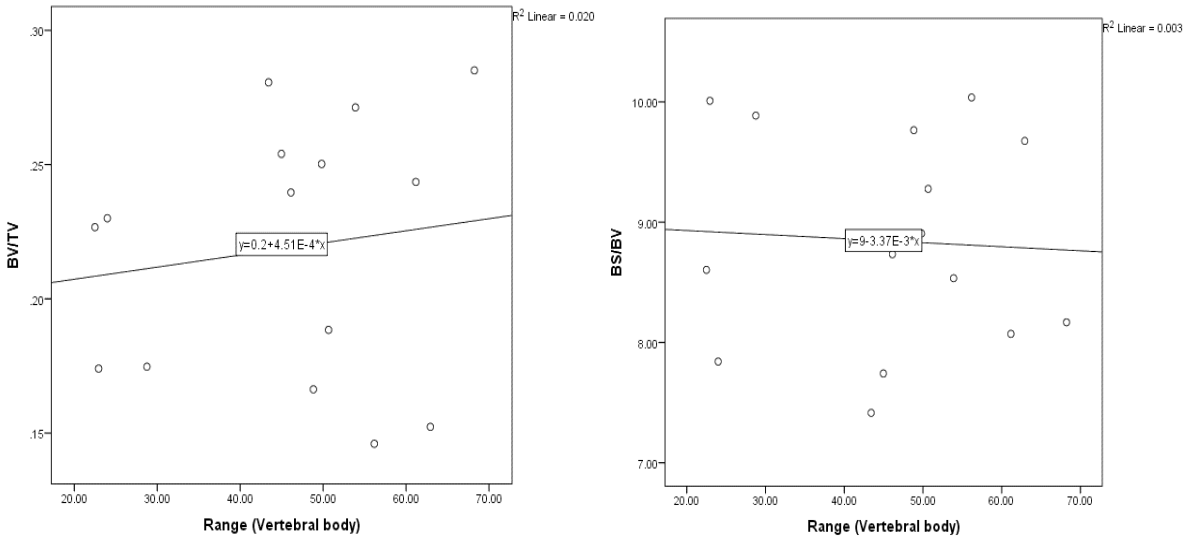

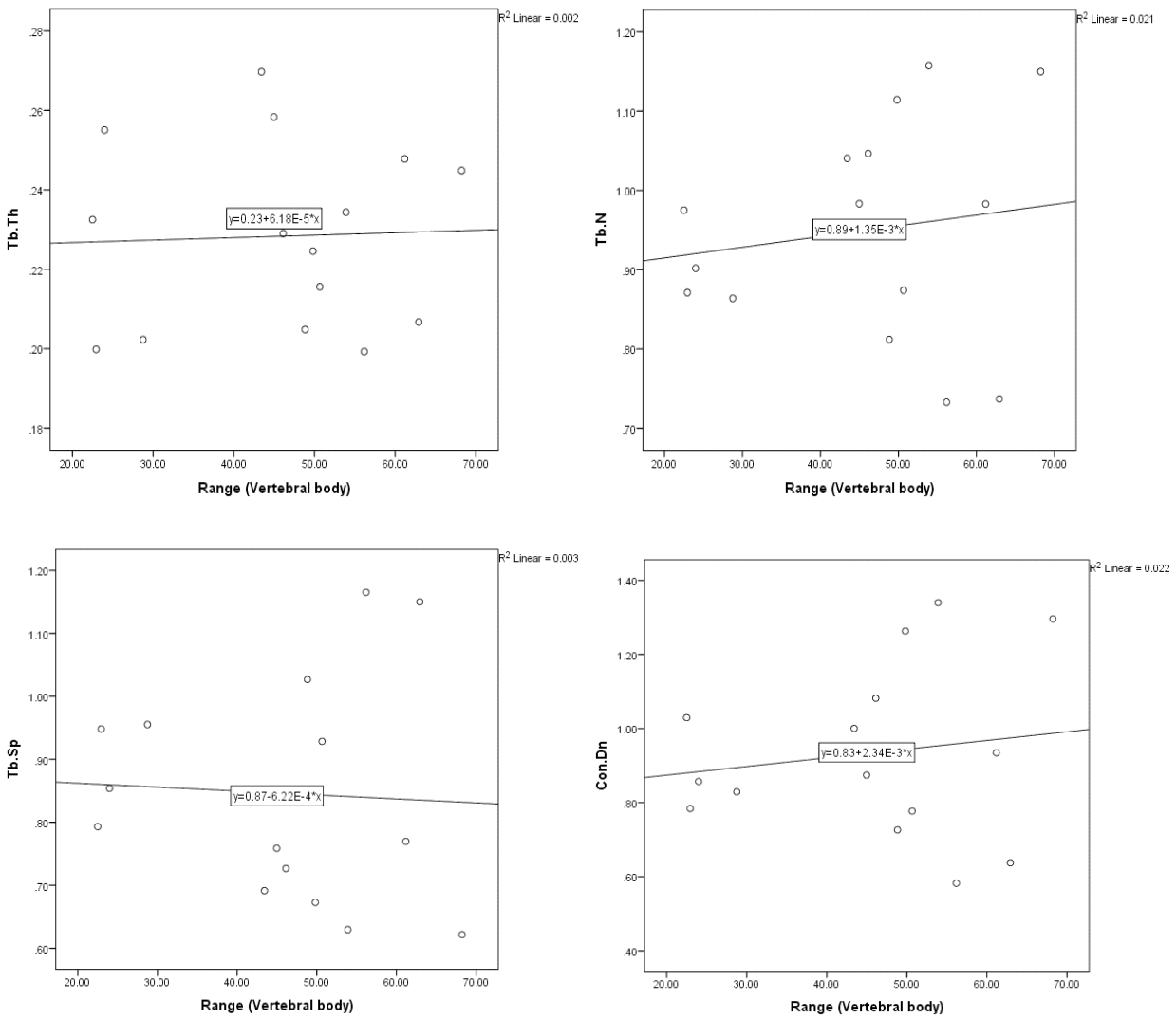

Figure 8. Linear regression analysis of Range of the vertebral body and bone volume fraction, bone surface to volume ratio, Trabecular thickness, Trabecular number, Trabecular separation, and connectivity density.

The range of the vertebral body was positively correlated with the bone volume fraction and a mild positive correlation is seen with the trabecular thickness, trabecular number, and connectivity density. It was negatively correlated with the bone surface-to-volume ratio and trabecular separation.

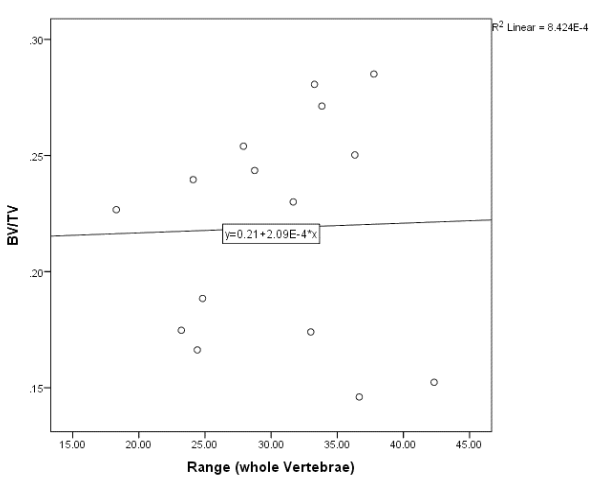
R² Linear = 8.424E-4
BV/TV
y=0.21+2.09E-4*x
Range (whole Vertebrae)

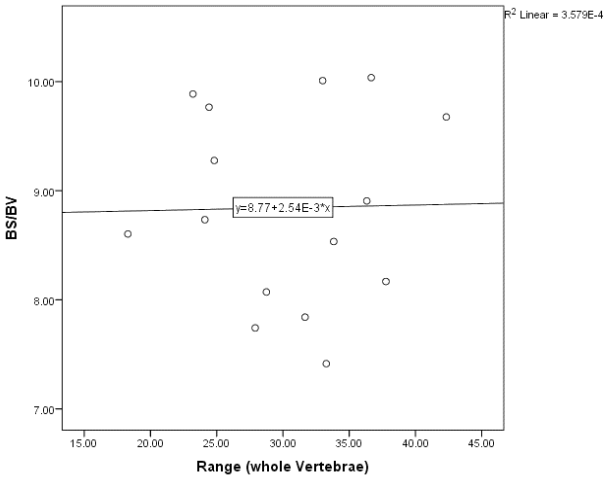
R² Linear = 3.579E-4
BS/BV
y=8.77+2.54E-3*x
Range (whole Vertebrae)

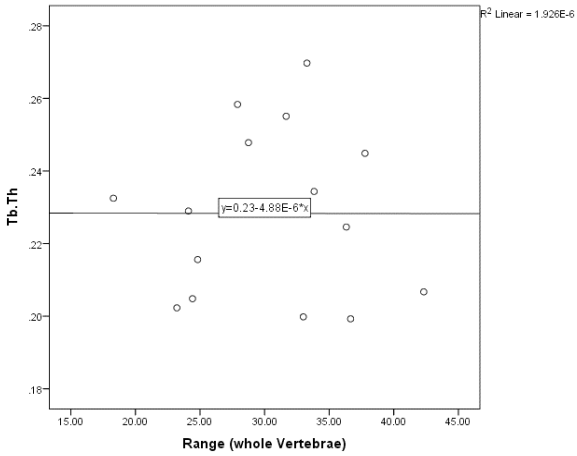
R² Linear = 1.926E-6
Tb.Th
y=0.23-4.88E-6*x
Range (whole Vertebrae)

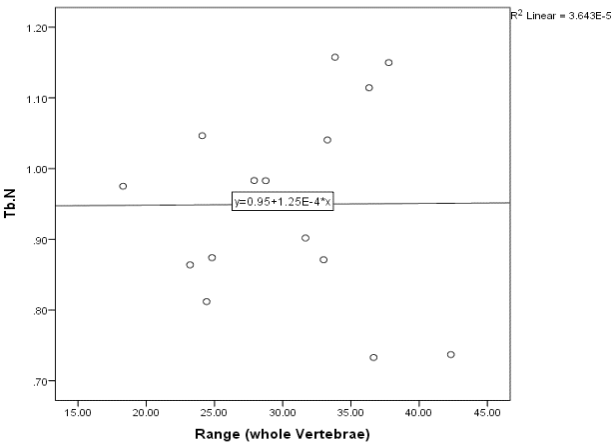
R² Linear = 3.643E-5
Tb.N
y=0.95+1.25E-4*x
Range (whole Vertebrae)

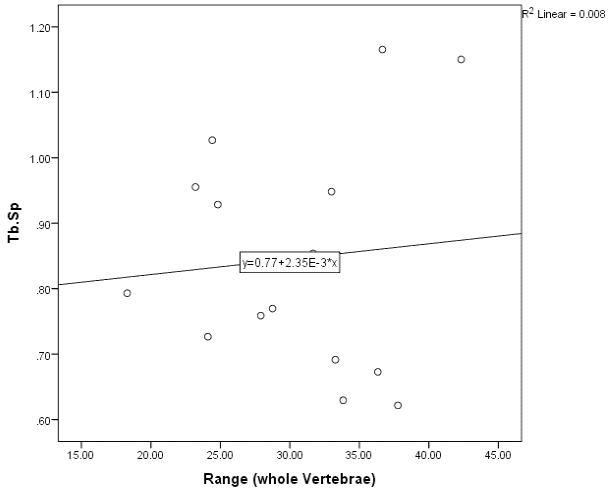
R² Linear = 0.008
Tb.Sp
y=0.77+2.35E-3*x
Range (whole Vertebrae)

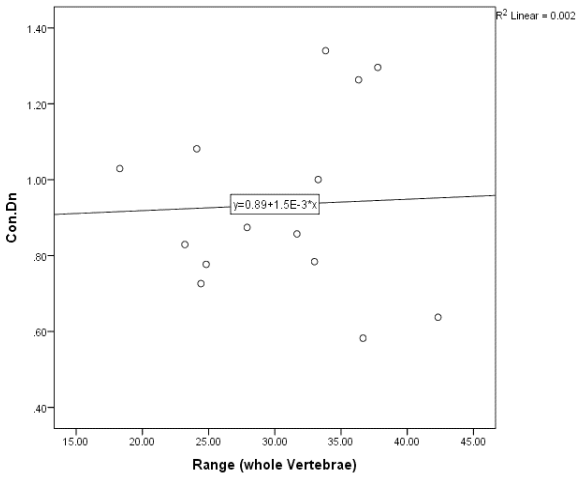
R² Linear = 0.002
Con.Dn
y=0.89+1.5E-3*x
Range (whole Vertebrae)

Figure 9. Linear regression analysis of Range of whole vertebrae and bone volume fraction, the bone surface to volume ratio, Trabecular thickness, Trabecular number, Trabecular separation, and connectivity density.

The range of whole vertebrae was positively correlated with the bone volume fraction, the bone surface to volume ratio, trabecular number, trabecular separation, and connectivity density. It was not correlated with the trabecular thickness.

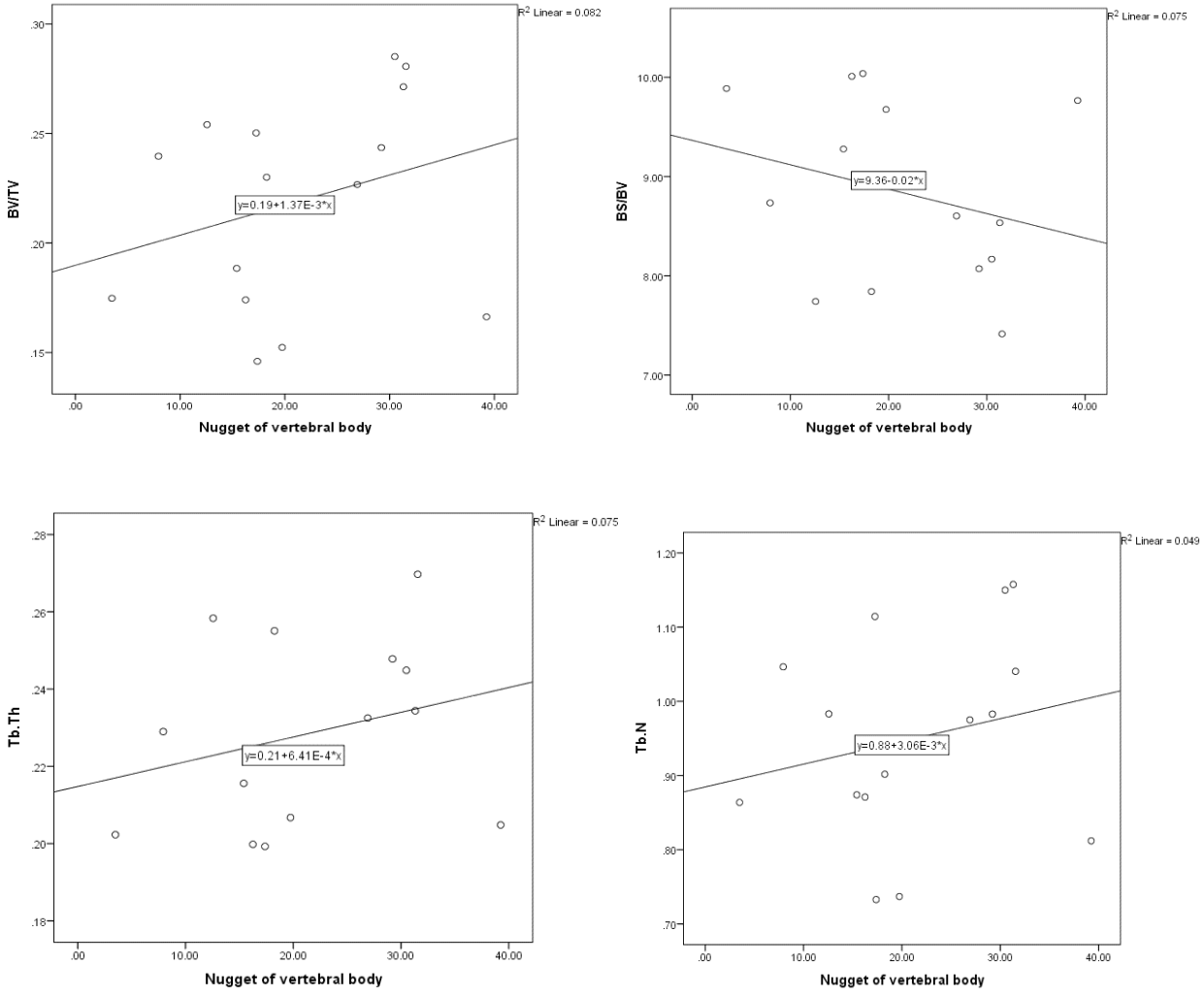

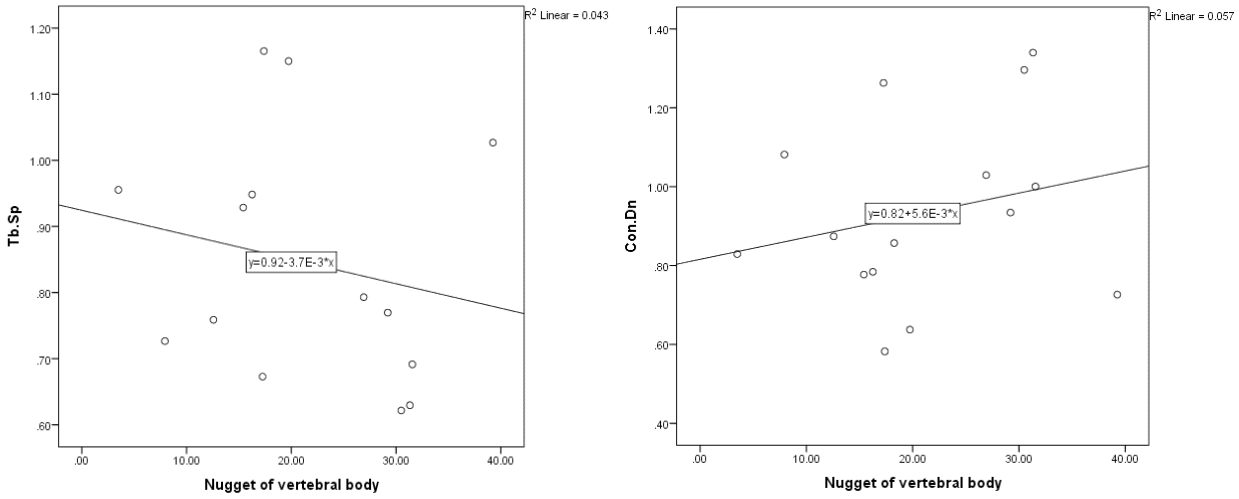

Figure 10. Linear regression analysis of Nugget of the vertebral body and bone volume fraction, bone surface to volume ratio, Trabecular thickness, Trabecular number, Trabecular separation, and connectivity density.

The nugget of the vertebral body was positively correlated with the bone volume fraction, trabecular thickness, trabecular number, and connectivity density. It was negatively correlated with the bone surface-to-volume ratio, trabecular separation.

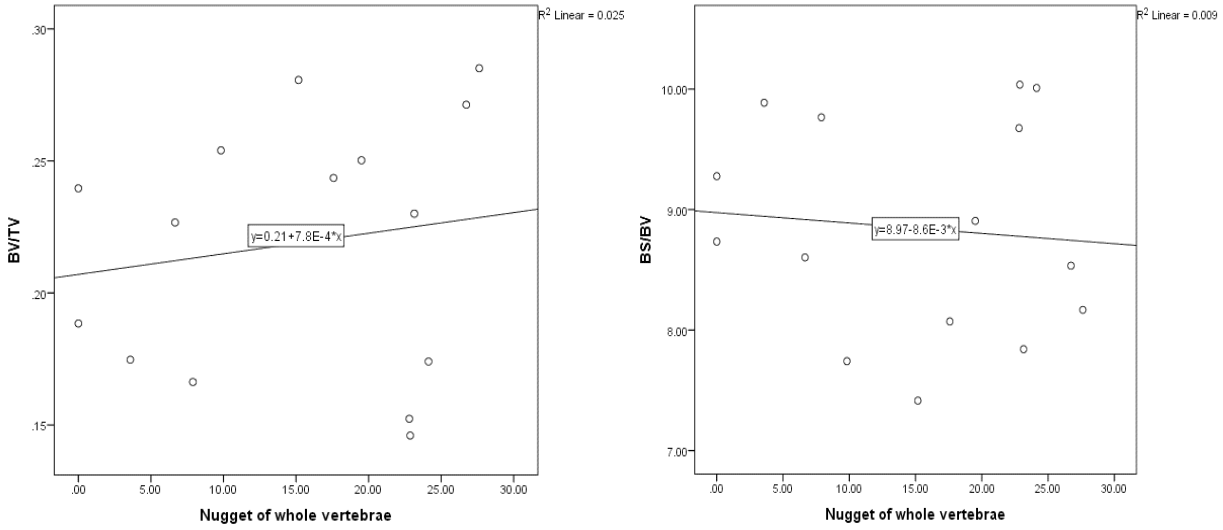

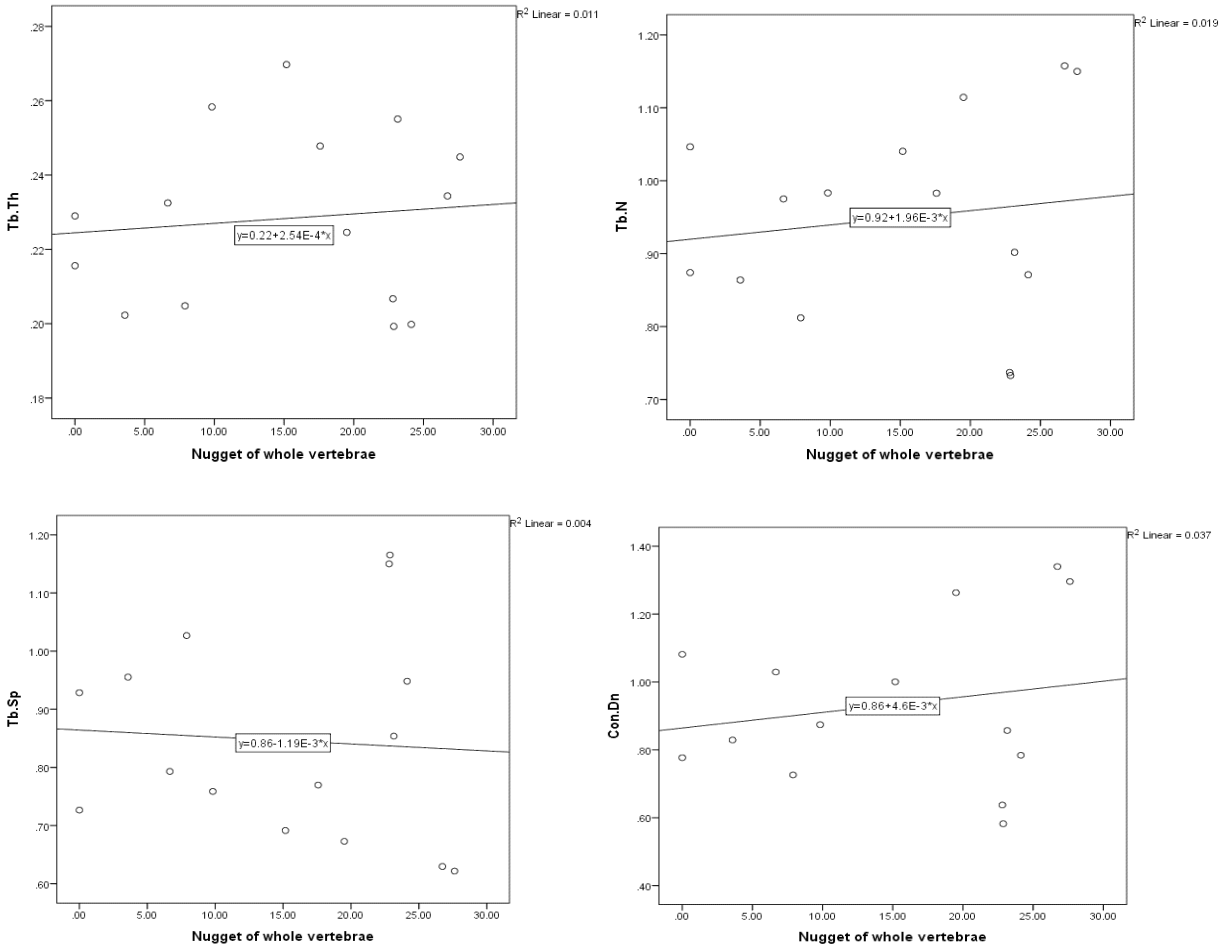

Figure 11. Linear regression analysis of nugget of the whole vertebrae and bone volume fraction, bone surface to volume ratio, trabecular thickness, trabecular number, trabecular separation, and connectivity density.

The nugget of whole vertebrae was positively correlated with the bone volume fraction, trabecular thickness, trabecular number, and connectivity density. It was negatively correlated with the bone surface-to-volume ratio and trabecular separation.

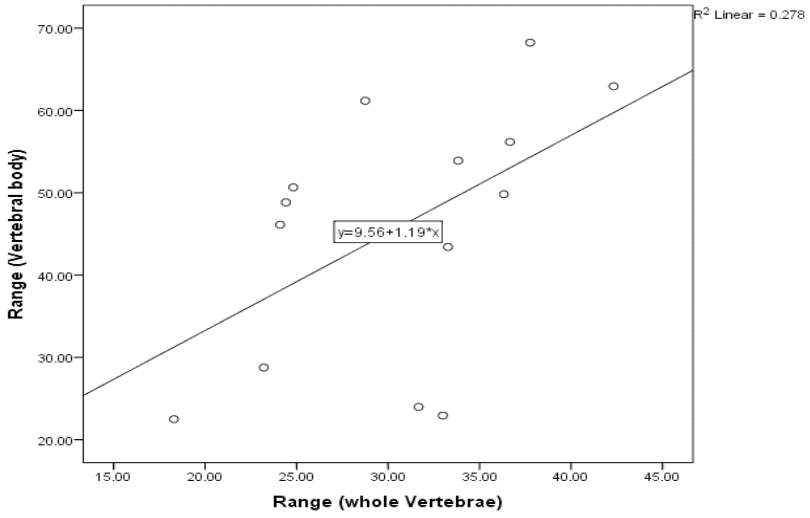

Figure 12. Linear regression analysis of the Range of whole vertebrae and Range of the vertebral body. The Range of whole vertebrae was positively correlated with the Range of the vertebral body with a coefficient of determination (R^2 =0.278).

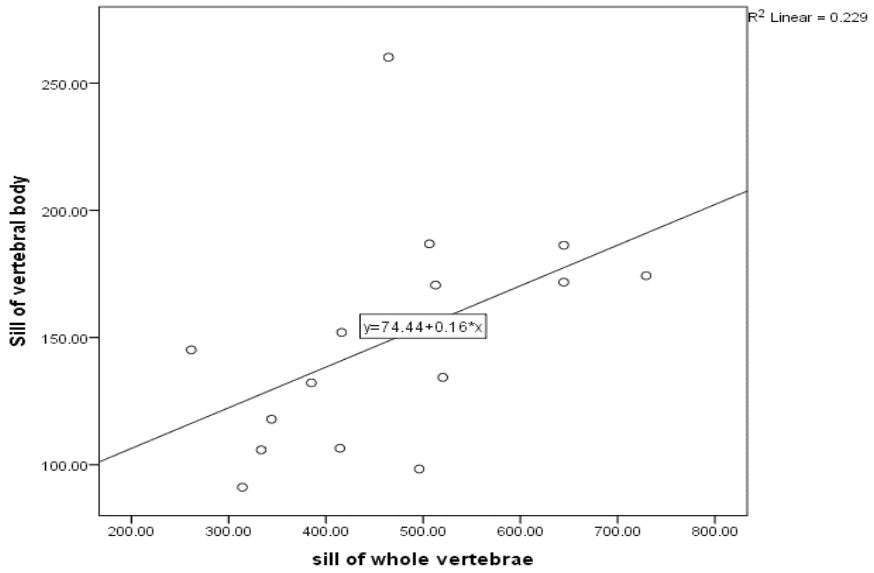

Figure 13. Linear regression analysis of Sill variance of whole vertebrae and Sill variance of the vertebral body. The Sill variance of whole vertebrae was positively correlated with the Sill variance of a vertebral body with a coefficient of determination (R^2 =0.229).

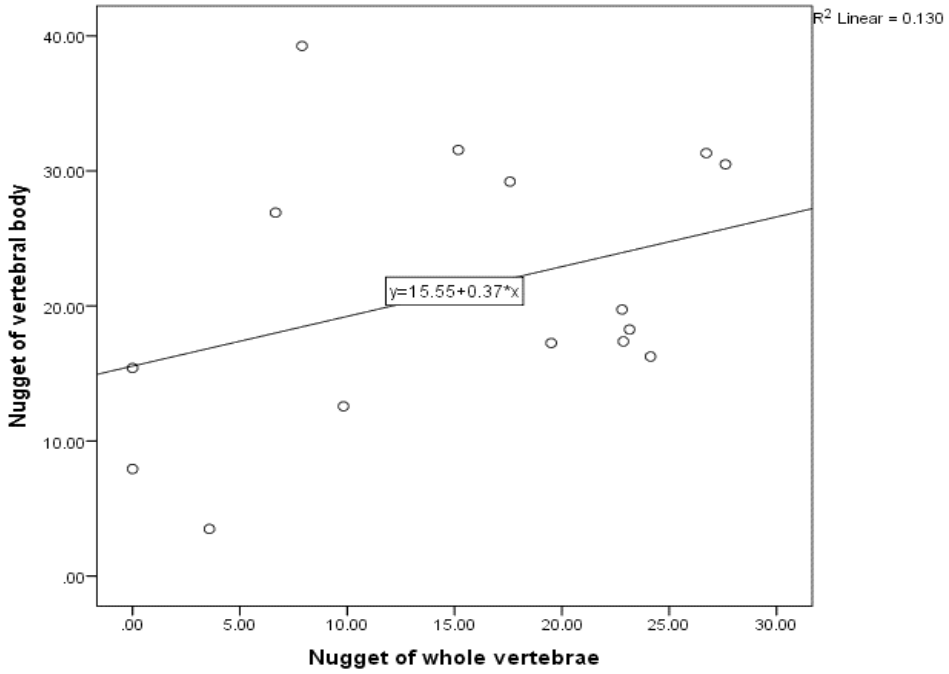

Figure 14. Linear regression analysis of Nugget of whole vertebrae and Nugget of the vertebral body. The Nugget of whole vertebrae was positively correlated with the Nugget of vertebral body with a coefficient of determination (R^2 =0.130).

Chapter 5

Discussion and Conclusions

In this study, eighteen human vertebrae with intact posterior elements were scanned by the Micro-CT scanner. Then, the MicroCT images were imported into *Microview* to measure microarchitecture parameters. Additionally, simulated DXA images with and without posterior elements were generated from 3D MicroCT images of human lumbar vertebrae. Stochastic parameters such as correlation length, sill variance, and nugget variable were calculated by fitting a theoretical model onto the experimental variogram of simulated DXA images with and without posterior elements. The main outcome was to identify the correlations between stochastic predictors and microarchitecture parameters for simulated DXA images with and without posterior elements.

The sill variance of simulated DXA images without posterior elements was positively correlated with some of the microarchitecture parameters such as bone surface to volume ratio, trabecular separation, and negatively correlated with bone volume fraction, trabecular thickness, trabecular number. The sill variance of simulated DXA images of whole vertebrae was positively correlated with bone volume fraction, trabecular thickness, trabecular number, and connectivity density, and negatively correlated with the bone surface to volume ratio, trabecular separation. However, these correlations were not statistically significant. In the previous study of 2D projection images generated from 3D Micro-CT images of trabecular bone, we have observed that the sill variance was positively correlated with bone volume fraction, trabecular thickness, and trabecular number, but negatively correlated with the bone surface to volume ratio and bone separation (Dong et al., 2013). This finding is consistent with our findings in the current study. But the sill variance of simulated DXA images without posterior elements in the current study was not in agreement with

the previous study. A positive relationship between sill variance and trabecular thickness and the negative relationship between sill variance and trabecular separations indicated that decreases in bone heterogeneity led to increases in bone fragility (Burr, 2003).

The range of simulated DXA images without posterior elements are positively correlated with bone volume fraction, trabecular thickness, trabecular number, connectivity density, and negatively correlated with the bone surface to volume ratio, trabecular separation. The range of simulated DXA images of whole vertebrae is minimally correlated with bone volume fraction, the bone surface to volume ratio, trabecular number, trabecular separation, connectivity density. But these correlations did not reach a statistically significant level. This may be because of the small sample size and the procedures in simulating DXA images. It is noted that the effect size of linear regression analysis between sill variance and trabecular thickness of vertebral bodies without posterior elements was the medium effect (f^2=0.26).

In this study, significant correlations between stochastic predictors and microarchitecture parameters were not observed for simulated DXA images of human vertebrae with and without posterior elements. However, the correlations between the sill variance and the microarchitecture parameters were mostly higher in the vertebral bodies without posterior elements than in the whole vertebrae with intact posterior elements. It suggests that the removal of posterior elements will likely enhance the prediction of microarchitecture parameters from stochastic predictors of simulated DXA images. This may provide us with the rationale to remove posterior elements from clinical DXA scans.

Limitations and future work

This study has several limitations that can be addressed in future work. First, the number of subjects (cadavers' spines) used in this study is small, even though the total number of vertebral

specimens is eighteen. Second, the use of Image J software may have an issue with the precision of simulating the DXA images from 3D micro-CT scans. Third, low resolution (92 μm) micro-CT images of specimens are used. This suggests that the accuracy of measuring microarchitecture parameters of trabecular bone can be improved using high-resolution (20 μm) micro-CT images. Fourth, gender differences couldn't be established in this study. The last one is the stochastic predictors can be influenced by scanner noise, mode, and resolution, and also by any structural artifacts like osteophytes. Therefore, future studies can take this all into consideration.

Future Directions

This study suggests that the removal of posterior elements from clinical DXA scans of the human lumbar spine will improve the power of stochastic predictors in enhancing the prediction of bone fragility. Therefore, our future directions are to use independent component analysis to remove posterior elements from clinical DXA scans. In addition, we can also explore the possibility of machine learning in removing the posterior elements from clinical DXA scans of the human lumbar spine.

REFERENCES

Ackerman, K., Pierce, L., Guereca, G., Slattery, M., Lee, H., Goldstein, M., & Misra, M. (2013). Hip structural analysis in adolescent and young adult oligoamenorrheic and eumenorrheic athletes and nonathletes. *The Journal of clinical endocrinology and metabolism, 98 4*, 1742-1749.

Anderson, D. E., Demissie, S., Allaire, B. T., Bruno, A. G., Kopperdahl, D. L., Keaveny, T. M., Kiel, D. P., & Bouxsein, M. L. (2014). The associations between QCT-based vertebral bone measurements and prevalent vertebral fractures depend on the spinal locations of both bone measurement and fracture. *Osteoporosis international : a journal established as result of cooperation between the European Foundation for Osteoporosis and the National Osteoporosis Foundation of the USA, 25*(2), 559. https://doi.org/10.1007/s00198-013-2452-0

Atkinson, P. M., & Lloyd, C. D. (2007). Non-stationary variogram models for geostatistical sampling optimisation: An empirical investigation using elevation data. *Computers & geosciences, 33*(10), 1285-1300. https://doi.org/10.1016/j.cageo.2007.05.011

Bjarnason, K., Hassager, C., Svendsen, O. L., Stang, H., & Christiansen, C. (2005). Anteroposterior and lateral spinal DXA for the assessment of vertebral body strength: Comparison with hip and forearm measurement. *Osteoporosis International, 6*, 37-42.

Bolotin, H. H., & Sievänen, H. (2001). Inaccuracies Inherent in Dual-Energy X-Ray Absorptiometry In Vivo Bone Mineral Density Can Seriously Mislead Diagnostic/Prognostic Interpretations of Patient-Specific Bone Fragility. *Journal of Bone and Mineral Research, 16*(5), 799-805. https://doi.org/10.1359/jbmr.2001.16.5.799

Bonnick, S. L. (2012). *Bone Densitometry for Technologists* (3rd ed.. ed.). Dordrecht : Springer.

Bouxsein, M. (2003). Bone quality: where do we go from here? *Osteoporosis International, 14*(S5), S118-127. https://doi.org/10.1007/s00198-003-1489-x

Burge, R., Dawson-Hughes, B., Solomon, D. H., Wong, J. B., King, A., & Tosteson, A. (2007). Incidence and Economic Burden of Osteoporosis-Related Fractures in the United States, 2005–2025. *Journal of Bone and Mineral Research, 22*(3), 465-475. https://doi.org/10.1359/jbmr.061113

Burr, D. (2003). Microdamage and bone strength. *Osteoporosis International, 14*(9), 67.

Ciarelli, M. J., Goldstein, S. A., Kuhn, J. L., Cody, D. D., & Brown, M. B. (1991). Evaluation of orthogonal mechanical properties and density of human trabecular bone from the major metaphyseal regions with materials testing and computed tomography. *Journal of Orthopaedic Research, 9*(5), 674-682. https://doi.org/10.1002/jor.1100090507

Dong, X. N., Lu, Y., Krause, M., Huber, G., Chevalier, Y., Leng, H., & Maquer, G. (2018). Variogram-based evaluations of DXA correlate with vertebral strength, but do not enhance the prediction compared to aBMD alone. *Journal of biomechanics, 77*, 223-227. https://doi.org/10.1016/j.jbiomech.2018.07.009

Dong, X. N., Pinninti, R., Lowe, T., Cussen, P., Ballard, J. E., Di Paolo, D., & Shirvaikar, M. (2015). Random field assessment of inhomogeneous bone mineral density from DXA scans can enhance the differentiation between postmenopausal women with and without hip fractures. *Journal of biomechanics, 48*(6), 1043-1051. https://doi.org/10.1016/j.jbiomech.2015.01.030

Dong, X. N., Pinninti, R., Tvinnereim, A., Lowe, T., Di Paolo, D., & Shirvaikar, M. (2015). Stochastic predictors from the DXA scans of human lumbar vertebrae are correlated with the microarchitecture parameters of trabecular bone. *Journal of biomechanics*, *48*(12), 2968-2975. https://doi.org/10.1016/j.jbiomech.2015.07.041

Dong, X. N., Shirvaikar, M., & Wang, X. (2013). Biomechanical properties and microarchitecture parameters of trabecular bone are correlated with stochastic measures of 2D projection images. *Bone (New York, N.Y.)*, *56*(2), 327-336. https://doi.org/10.1016/j.bone.2013.05.023

Gokalp, G., Mutlu, F. S., Yazici, Z., & Yildirim, N. (2011). Evaluation of vertebral bone marrow fat content by chemical-shift MRI in osteoporosis. *Skeletal radiology*, *40*(5), 577-585. https://doi.org/10.1007/s00256-010-1048-4

Kanis, J. A., Harvey, N. C., Johansson, H., Odén, A., McCloskey, E. V., & Leslie, W. D. (2017). Overview of Fracture Prediction Tools. *Journal of clinical densitometry*, *20*(3), 444-450. https://doi.org/10.1016/j.jocd.2017.06.013

Kazakia, G., & Majumdar, S. (2006). New imaging technologies in the diagnosis of osteoporosis. *Reviews in Endocrine & Metabolic Disorders*, *7*(1-2), 67-74. https://doi.org/10.1007/s11154-006-9004-2

Koyama, H., Yoshihara, H., Kotera, M., Tamura, T., & Sugimura, K. (2013). The quantitative diagnostic capability of routine MR imaging and diffusion-weighted imaging in osteoporosis patients. *Clinical imaging*, *37*(5), 925-929. https://doi.org/10.1016/j.clinimag.2013.05.001

Krug, R., Banerjee, S., Han, E. T., Newitt, D. C., Link, T. M., & Majumdar, S. (2005). Feasibility of in vivo structural analysis of high-resolution magnetic resonance images of the proximal femur.(REVIEW)(Clinical report). *Osteoporosis International*, *16*(11), 1307. https://doi.org/10.1007/s00198-005-1907-3

Lee, D., Campbell, P., Gilsanz, V., & Wren, T. (2009). Contribution of the Vertebral Posterior Elements in Anterior-Posterior DXA Spine Scans in Young Subjects. *Journal of Bone and Mineral Research*, *24*(8), 1398-1403. https://doi.org/10.1359/JBMR.090224

Lewiecki, E. M., Gordon, C. M., Baim, S., Leonard, M. B., Bishop, N. J., Bianchi, M.-L., Kalkwarf, H. J., Langman, C. B., Plotkin, H., Rauch, F., Zemel, B. S., Binkley, N., Bilezikian, J. P., Kendler, D. L., Hans, D. B., & Silverman, S. (2008). International Society for Clinical Densitometry 2007 Adult and Pediatric Official Positions. *Bone (New York, N.Y.)*, *43*(6), 1115-1121. https://doi.org/10.1016/j.bone.2008.08.106

Marshall, D., Johnell, O., & Wedel, H. (1996). Meta-Analysis Of How Well Measures Of Bone Mineral Density Predict Occurrence Of Osteoporotic Fractures. *BMJ: British Medical Journal*, *312*(7041), 1254-1259. https://doi.org/10.1136/bmj.312.7041.1254

Moyad, M. A. (2003). Osteoporosis: a rapid review of risk factors and screening methods. *Urologic oncology*, *21*(5), 375-379. https://doi.org/10.1016/S1078-1439(03)00140-6

Myers, E. R., & Wilson, S. E. (1997). Biomechanics of osteoporosis and vertebral fracture. *Spine (Phila Pa 1976)*, *22*(24 Suppl), 25s-31s. https://doi.org/10.1097/00007632-199712151-00005

Nanes, M. S., & Kallen, C. B. (2014). Osteoporosis. *Seminars in nuclear medicine*, *44*(6), 439-450. https://doi.org/10.1053/j.semnuclmed.2014.06.006

Nishiyama, K. K., & Shane, E. (2013). Clinical Imaging of Bone Microarchitecture with HR-pQCT.(Report). *Current Osteoporosis Reports*, *11*(2), 147. https://doi.org/10.1007/s11914-013-0142-7

Oei, L., Koromani, F., Rivadeneira, F., Zillikens, M. C., & Oei, E. H. G. (2016). Quantitative imaging methods in osteoporosis. *Quantitative imaging in medicine and surgery*, *6*(6), 680-698. https://doi.org/10.21037/qims.2016.12.13

Office of the Surgeon, G. (2004). Reports of the Surgeon General. In *Bone Health and Osteoporosis: A Report of the Surgeon General*. Office of the Surgeon General (US).

Osteoporosis : cause, treatment, prevention / [prepared by the National Institute of Arthritis and Musculoskeletal and Skin Diseases, National Institutes of Health]. (1986). U.S. Dept. of Health and Human Services, Public Health Service, National Institutes of Health.

Pinninti, R. R. (2015). Stochastic Assessment of Bone Fragility in Human Lumbar Spine. In: Scholar Works at UT Tyler.

Ramos, R. (2016). PRECISION STUDY OF STOCHASTIC PREDICTORS FOR DXA SCANS. In: Scholar Works at UT Tyler.

Rosen, C. J. (2013). *Primer on the Metabolic Bone Diseases and Disorders of Mineral Metabolism* (8th ed.. ed.). Hoboken : Wiley.

Rosen, H. N., Vokes, T. J., Malabanan, A. O., Deal, C. L., Alele, J. D., Olenginski, T. P., & Schousboe, J. T. (2013). The Official Positions of the International Society for Clinical Densitometry: Vertebral Fracture Assessment. *Journal of clinical densitometry*, *16*(4), 482-488. https://doi.org/10.1016/j.jocd.2013.08.003

Silva, B. C., Leslie, W. D., Resch, H., Lamy, O., Lesnyak, O., Binkley, N., McCloskey, E. V., Kanis, J. A., & Bilezikian, J. P. (2014). Trabecular Bone Score: A Noninvasive Analytical Method Based Upon the DXA Image. *Journal of Bone and Mineral Research*, *29*(3), 518-530. https://doi.org/10.1002/jbmr.2176

Sozen, T., Ozisik, L., & Basaran, N. C. (2017). An overview and management of osteoporosis.(Report). *European Journal of Rheumatology*, *4*(1), 46. https://doi.org/10.5152/eurjrheum.2016.048

Tella, S. H., & Gallagher, J. C. (2014). Prevention and treatment of postmenopausal osteoporosis. *The Journal of steroid biochemistry and molecular biology*, *142*, 155-170. https://doi.org/10.1016/j.jsbmb.2013.09.008

Wang, Y., Videman, T., Boyd, S. K., & Battié, M. C. (2015). The distribution of bone mass in the lumbar vertebrae: are we measuring the right target? *The spine journal*, *15*(11), 2412-2416. https://doi.org/10.1016/j.spinee.2015.06.059

Whitmarsh, T., Humbert, L., Del Río Barquero, L. M., Di Gregorio, S., & Frangi, A. F. (2013). 3D reconstruction of the lumbar vertebrae from anteroposterior and lateral dual-energy X-ray absorptiometry. *Medical image analysis*, *17*(4), 475-487. https://doi.org/10.1016/j.media.2013.02.002

Wright, N. C., Looker, A. C., Saag, K. G., Curtis, J. R., Delzell, E. S., Randall, S., & Dawson-Hughes, B. (2014). The Recent Prevalence of Osteoporosis and Low Bone Mass in the United States Based on Bone Mineral Density at the Femoral Neck or Lumbar Spine. *Journal of Bone and Mineral Research*, *29*(11), 2520-2526. https://doi.org/10.1002/jbmr.2269